MAGYAR ÁLLAMI
EÖTVÖS LORÁND
GEOFIZIKAI INTÉZET

EOTVOS LORÁND
GEOPHYSICAL INSTITUTE
OF HUNGARY

GEOFIZIKAI KÖZLEMÉNYEK

GEOPHYSICAL TRANSACTIONS

ВЕНГЕРСКИЙ
ГЕОФИЗИЧЕСКИЙ
ИНСТИТУТ
ИМ Л. ЭТВЕША

ГЕОФИЗИЧЕСКИЙ
БЮЛЛЕТЕНЬ

CONTENTS

Fast evaluation of radial and vertical magnetic field near a rectangular loop source on a layered earth	*W. L. Anderson*	339
Calculating galvanic anomalies for an inclined prism in a two-layered half-space	*H. Soininen*	359
A few unsolved problems of applied geophysics	*G. Korvin*	373
Frequency content of seismic waves as a function of charge	*H. Rische*	391
Computation and reliability of pseudo-porosity sections from seismic data	*I. Szulyovszky*	405

VOL. 31. NO. 4. DEC. 1985 (ISSN 0016–7177)

BUDAPEST

TARTALOM

A radiális és függőleges mágneses tér gyors számítása rétegzett földön fekvő, téglalap alakú hurokforrás közelében	*W. L. Anderson*	357
Kétréteges féltérben levő dőlt prizma galvanikus anomáliáinak számítása	*H. Soininen*	371
Az alkalmazott geofizika néhány megoldatlan problémája	*Korvin G.*	389
Szeizmikus hullámok frekvencia-tartalmának függése a töltetnagyságtól	*H. Rische*	403
Pszeudo-porozitás szelvények számítása szeizmikus adatokból és ezek megbízhatósága	*Szulyovszky I.*	417

СОДЕРЖАНИЕ

Быстрое вычисление радиального и вертикального магнитного поля вблизи возбуждающей петли прямоуголной формы, находящейся на поверхности слоистой среды	*В. Л. Андерсон*	357
Вычисление аномалий сопротивления и вызванной поляризации над наклонной призмой, вмещающей в двухслойной среде	*Х. Соининен*	371
Некоторые нерешенные проблемы прикладной геофизики	*Г. Корвин*	389
Зависимость частоты сейсмических волн от величины заряда	*Г. Рише*	403
Вычисление разрезов по сейсмическим данным псевдо-пористости и их надежность	*И. Суёвски*	417

GEOPHYSICAL TRANSACTIONS 1985
Vol. 31. No. 4. pp. 339–357

FAST EVALUATION OF RADIAL AND VERTICAL MAGNETIC FIELDS NEAR A RECTANGULAR LOOP SOURCE ON A LAYERED EARTH

Walter L. ANDERSON*

A fast Hankel transform (FHT) algorithm is used to compute simultaneously parametric (or geometric) soundings for radial and vertical magnetic fields inside or outside a rectangular loop source on the surface of a layered earth. The FHT uses concepts of related and lagged convolutions (linear digital filtering), and, when applied to the rectangular loop problem, reduces each field calculation to four elementary spline integrations. For parametric soundings, the FHT is called once for each frequency; for geometric soundings, only a single execution of the FHT is required to obtain both field components. Numerical comparisons of the FHT method with existing dipole, circular, and other rectangular loop forward solutions show that at least three-figure accuracy is achieved with greatly reduced computation time. Consequently, future inverse solutions in both frequency- and time-domains would become as practical for a rectangular loop as for a dipole source.

Keywords: electromagnetic methods, numerical modeling, frequency domain, layered model, Hankel transform

1. Introduction

Well known methods exist for calculating the electromagnetic (EM) fields at any distance from an oscillating vertical magnetic dipole or horizontal dipole source [e.g., FRISCHKNECHT 1967; WAIT 1958; WAIT 1966]. Linear digital filtering algorithms [e.g., ANDERSON 1979] provide rapid and accurate calculations for dipole sources. KAUAHIKAUA [1978] presented a method for computing the electric and magnetic field components about a straight horizontal finite-length grounded wire source over a layered earth. Recently, PODDAR [1983] developed the solution for the vertical magnetic field about a rectangular loop source of current on a multilayered earth. Poddar's solution used four separate double numerical integrations, and by superposition, obtained the total magnetic field inside or outside the rectangular loop at arbitrary positions. KRISTENSSON [1983] also presented a method of computing the EM field components in a layered earth for a general current distribution, including a horizontal rectangular loop source; his method, however, required direct evaluation of integrals and series involving Bessel functions.

The question of why a rectangular loop is specified here over a more general or arbitrary line segment loop naturally arises. BOERNER and WEST [1984]

* U.S. Geological Survey, Box 25046 M. S. 964, Denver Federal Center, Denver, Colorado 80225
Manuscript received: 10 June, 1985

presented an interesting method to compute efficiently the EM fields of an extended wire source. They suggested using the FHT algorithm (as proposed in the present paper, and published by ANDERSON, [1982]) to compute all Hankel transforms for a given field component by lagged convolution, and as required over all spatial distances for a given wire configuration. The total field is then computed by a weighted summation using weights derived from a precomputed quintic spline. However, the technique is often applied in practice to simple geometric sources that are easy to set up, such as a square or rectangular loop. This simplifies recording end-point coordinates in the measurement environment. Boerner and West's method is quite similar to my method, except they apparently proposed using it to compute only a single field component for each FHT execution.

This paper presents a new method to compute in one pass the radial (H_r) and vertical (H_z) magnetic fields about a rectangular loop source on a layered earth. The basic formulations for each field component reduce to four adaptive finite spline integrations, after first computing all related and lagged Hankel transforms using a single call to the FHT algorithm. Parametric (frequency) or geometric (distance) soundings for H_r and H_z can be computed at arbitrary points inside or outside the rectangular loop source of finite dimensions. The rectangular loop is assumed to be placed on the earth's surface and the layers are parallel to the surface. Displacement currents are neglected (quasi-static case) for all computations.

Recent advances in evaluating Hankel transforms by the FHT algorithm [ANDERSON 1982] lead naturally to this new approach, which extends PODDAR'S [1983] solution for H_z to include H_r (or simultaneously H_x and H_y) field components. This method is intended to provide a practical tool for studying the frequency response near the loop where a dipole source cannot be assumed. In most physical situations, it is easier to lay out a square or rectangular wire loop than a circular loop; consequently, this method should be more appropriate (and efficient) than an exclusively circular loop computation [e.g., RYU et al. 1970].

Some tests were made with small loop sizes and large spacings to simulate a dipole-dipole case. Both H_r and H_z results agreed to about 3-place accuracy with existing dipole source results [FRISCHKNECHT 1967]. Tests were also made using the same rectangular loop source and models as given by PODDAR [1983], which included H_r as well as H_z components; these results are discussed and illustrated in a following section.

A natural extension of the rectangular loop frequency-domain response to the time-domain can be made using a suitable Fourier transformation; e.g., see ANDERSON [1985], where only the H_z transient response is treated.

2. Theory and computations

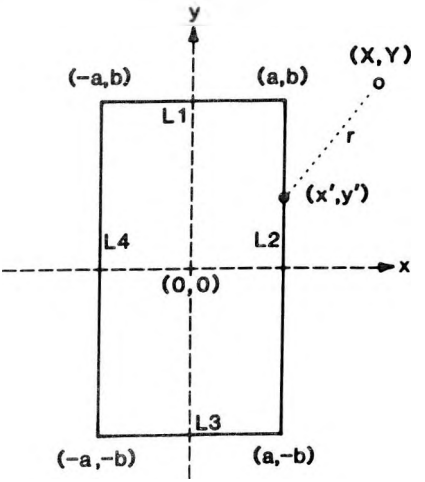

Fig. 1. Loop geometry at $z=0$ (earth's surface), where (X, Y) is the observation point, and (x', y') is any point on the rectangular loop source

1. ábra. A hurok geometriája $z=0$-nál (a föld felszínén), ahol (X, Y) a mérési pont és (x', y') a téglalap alakú hurokforrás tetszőleges pontja

Рис. 1. Геометрические данные контура. $z=0$ (поверхность земли), (X, Y) – точка измерения, (x', y') – любая точка прямоуголного контура

Figure 1 shows the coordinate system and geometry of a rectangular loop. Line segments $[(-a, b); (a, b)]$, $[(a, -b); (a, b)]$, $[(-a, -b); (a, -b)]$, and $[(-a, -b); (-a, b)]$ are denoted respectively as lines *L1*, *L2*, *L3*, and *L4*. The length of lines *L1* and *L3* is *2a*, and of lines *L2* and *L4* is *2b*.

The magnetic field inside or outside a rectangular loop can be formally obtained by a suitable summation of the results from four separate finite grounded wires as defined in KAUAHIKAUA [1978]. However, the rectangular loop problem is simpler, because there are no currents injected into the earth at the ends of each wire segment. The formulas in KAUAHIKAUA [1978] are written in a form such that the contribution from currents at the wire ends may be readily neglected; this fact will be used below in the H_r loop development. PODDAR [1983] derived his solution for a rectangular loop by starting with the electric field due to a magnetic dipole and then applying reciprocity. From PODDAR [1983], the vertical magnetic field H_z at any point (X, Y) for a loop source with current $I \exp(i\omega t)$ is

$$H_z = I(H_{L1} + H_{L2} + H_{L3} + H_{L4})/2\pi, \tag{1}$$

where

$$\begin{aligned}
H_{L1} &= -(b-Y) \int_{-a}^{a} (\mathrm{d}x'/r) \int_{0}^{\infty} k(\lambda)\, \mathrm{J}_1(\lambda \mathrm{r})\, \mathrm{d}\lambda, \qquad \mathrm{r}^2 = \mathrm{R}_1^2 \\
H_{L2} &= -(a-X) \int_{-b}^{b} (\mathrm{d}y'/r) \int_{0}^{\infty} k(\lambda)\, \mathrm{J}_1(\lambda \mathrm{r})\, \mathrm{d}\lambda, \qquad \mathrm{r}^2 = \mathrm{R}_2^2 \\
H_{L3} &= -(b+Y) \int_{-a}^{a} (\mathrm{d}x'/r) \int_{0}^{\infty} k(\lambda)\, \mathrm{J}_1(\lambda \mathrm{r})\, \mathrm{d}\lambda, \qquad \mathrm{r}^2 = \mathrm{R}_3^2 \\
H_{L4} &= -(a+X) \int_{-b}^{b} (\mathrm{d}y'/r) \int_{0}^{\infty} k(\lambda)\, \mathrm{J}_1(\lambda \mathrm{r})\, \mathrm{d}\lambda, \qquad \mathrm{r}^2 = \mathrm{R}_4^2
\end{aligned} \tag{2}$$

$$\begin{aligned} R_1^2 &= (x'-X)^2+(b-Y)^2, \\ R_2^2 &= (a-X)^2+(y'-Y)^2, \\ R_3^2 &= (x'-X)^2+(b+Y)^2, \\ R_4^2 &= (a+X)^2+(y'-Y)^2, \end{aligned} \tag{3}$$

and $k(\lambda)$ is a recursive complex kernel function [PODDAR 1983] containing the factor $\exp(-\lambda z)$, $z>0$. The Hankel transforms in equations (2) do not converge if the observation point is on the surface ($z=0$). To overcome this problem, Poddar set $z = 10^{-3}$ meters in $k(\lambda, z)$. This approach was not used in this paper, because some advantage is gained using $z=0$ and the fast converging formulas derived by KAUAHIKAUA [1978]. Here the half-space response was removed from $k(\lambda)$ and a closed-form expression added outside the integrals. This modification to equations (2) becomes

$$\begin{aligned} H_{L1} &= -(b-Y)\int_{-a}^{a} (\mathrm{d}x'/r)\{h_z^S(r)\}, \quad r^2 = R_1^2 \text{ in (3)} \\ H_{L2} &= -(a-X)\int_{-b}^{b} (\mathrm{d}y'/r)\{h_z^S(r)\}, \quad r^2 = R_2^2 \text{ in (3)} \\ H_{L3} &= -(b+Y)\int_{-a}^{a} (\mathrm{d}x'/r)\{h_z^S(r)\}, \quad r^2 = R_3^2 \text{ in (3)} \\ H_{L4} &= -(a+X)\int_{-b}^{b} (\mathrm{d}y'/r)\{h_z^S(r)\}, \quad r^2 = R_4^2 \text{ in (3)}, \end{aligned} \tag{4}$$

where

$$h_z^S(r) = \frac{1}{\delta}\int_0^{\infty} f_4(\lambda\delta)\, J_1(\lambda r)\,\mathrm{d}\lambda - \mathrm{i}\,\delta\,[h_z^0(B)]/(2r^4), \tag{5}$$

$$h_z^0(B) = 3-\{3+3B(1+i)+2iB^2\}\exp[-(1+i)B], \quad i=(-1)^{1/2},$$

$$B = r/\delta, \quad \delta = [2/(\sigma_1\mu_0\omega)]^{1/2}, \quad \omega = 2\pi f, \quad f>0 \text{ frequency (Hertz)},$$

$$\sigma_1 = \text{conductivity of layer 1 (Siemens/m)},$$

$$\mu_0 = 4\pi 10^{-7} \text{ permeability of free space (Weber/Am)},$$

and

$f_4(\lambda\delta)$ is defined in KAUAHIKAUA [1978] as $f_4(g)$.

(The complex recursive expressions used in $f_4(g)$ and all associated formulas and notations are explicitly listed in KAUAHIKAUA [1978, p. 1019–1021], and will not be repeated here; note that $f_4(g)$ contains all the parameters defining the layered earth model.)

Equation (5) is a continuous complex function defined for all r in $[r_{min}, r_{max}]$, where r_{min} and r_{max} are the respective minimum and maximum values of distances from (X, Y) to all points on the rectangular loop. The Hankel transform and

other expressions in equation (5) are in general required over different subintervals of r for each definite integral in equations (4). If equation (5) is sufficiently discretized over all r in $[r_{min}, r_{max}]$, then a single predetermined spline interpolating function (denoted by superscript S) can be used instead of equation (5) directly for each definite integral. Thus the four double integrations in equations (2) are essentially replaced by four single spline integrations in equations (4). The Hankel transform evaluations in equation (5), coupled with a lagged convolution (or discretation) over all r in $[r_{min}, r_{max}]$, is greatly facilitated by using the FHT algorithm, which is the principal reason for the fast computation times possible using equation (5). Once equation (5) is precomputed by lagged convolution and saved for all r in $[r_{min}, r_{max}]$, then equations (4) can be evaluated by elementary spline integration [ALBERG et al., 1967, p. 44], or by adaptive Gaussian quadrature [PATTERSON 1973] using a spline-defined integrand. Note that the above procedure must be repeated for each new frequency for parametric soundings, but only a *single* execution of the FHT is needed for geometric soundings.

The H_r radial field component is derived by analogy with H_z above, using the formula for $H_y^{f_{in}}$ in KAUAHIKAUA [1978], but neglecting the term due to the wire ends. The H_r field at any point (X, Y) becomes,

$$H_r = H_x(X/R_0) + H_y(Y/R_0), \qquad R_0^2 = X^2 + Y^2, \tag{6}$$

where

$$\begin{aligned}
H_x &= I(-h_{L2} + h_{L4})/2\pi, & H_y &= I(-h_{L1} + h_{L3})/2\pi,\\
h_{L1} &= -\int_{-a}^{a} (\mathrm{d}x'/r)\{h_r^S(r)\}, & r^2 &= R_1^2 \text{ in (3)}\\
h_{L2} &= -\int_{-b}^{b} (\mathrm{d}y'/r)\{h_r^S(r)\}, & r^2 &= R_2^2 \text{ in (3)}\\
h_{L3} &= -\int_{-a}^{a} (\mathrm{d}x'/r)\{h_r^S(r)\}, & r^2 &= R_3^2 \text{ in (3)}\\
h_{L4} &= -\int_{-b}^{b} (\mathrm{d}y'/r)\{h_r^S(r)\}, & r^2 &= R_4^2 \text{ in (3)},
\end{aligned} \tag{7}$$

$$\begin{aligned}
h_r^S(r) = -\{B\int_0^\infty f_4(\lambda\delta)\,J_0(\lambda r)\,\mathrm{d}\lambda + \frac{1}{r}[\beta(I_0(\beta)K_1(\beta) -\\
- I_1(\beta)K_0(\beta)) - 2I_1(\beta)K_1(\beta)]\},
\end{aligned} \tag{8}$$

$$\beta = B(1+i)/2, \qquad i = (-1)^{1/2},\ B = r/\delta,$$

and I_0, I_1, K_0, K_1 are modified Bessel functions of orders 0 and 1.

Equation (8) is replaced by a precomputed spline function analogous to equation (5). Modified Bessel functions are needed initially in equation (8) to compute the spline coefficients, but they are not required while performing the four spline integrations in equations (7).

Computation of all H_z and H_r Hankel transforms required in equations (5) and (8) are obtained rapidly by the FHT algorithm using related and lagged convolutions [ANDERSON 1982]. Observe that both Hankel transforms in equations (5) and (8) have the same kernel function $f_4(\lambda\delta)$, but have different order Bessel functions. The FHT algorithm was developed to integrate in parallel both orders 0 and 1 for any arbitrary transform argument range by lagged convolution, and to simultaneously provide for algebraically related kernels (in this case, the kernels are identical). Thus, with *one* execution of the FHT algorithm, a complete 2-column matrix of Hankel transforms (orders 0 and 1) is computed over a small digitized interval in r equivalent to the digital filter sampling interval (specifically, 0.2 in log-space). Therefore, both H_r and H_z field components are obtained in nearly the same time as would be required to evaluate a single component. Optionally, the H_x and H_y orthogonal components at (X, Y) can be computed instead of H_r. Observe from equation (6) that $H_r = H_x$ if $Y=0$, and $H_r = H_y$ if $X=0$.

The Hankel transforms in equations (5) and (8) are zero for a half-space model, which is one benefit of using the $z=0$ formulas from KAUAHIKAUA [1978], instead of the $z>0$ case of PODDAR [1983]. The general expressions in equations (5) and (8) apply to either parametric or geometric soundings, thus providing a unified mathematical treatment.

3. Computer program

A computer program (HRZRECT) that implements the algorithm presented in this paper is documented in ANDERSON [1984]. The code was written in FORTRAN–77 for a VAX–11/780 VMS system, and is listed in ANDERSON [1984].

4. Examples and discussion

Examples of soundings for various models computed using program HRZRECT are summarized graphically in this section. Numerical results and VAX execution times corresponding to these plots are tabulated in ANDERSON [1984]. Typically, complete geometric soundings for both H_r and H_z take about 2 to 5 CPU-seconds on the VAX computer. As would be expected, execution times are slightly larger for points very near the source. In general, it is recommended that (X, Y) should be chosen such that $r > \min(a, b)/10$ for all r. Usually, points very close to the source loop are of little practical interest, and should be avoided. Furthermore, a small saving is achieved in summing equations (1) and (6) whenever (X, Y) is chosen symmetrical with respect to the loop sides (e.g., $X>0$, $Y=0$).

The H_z results plotted in Figures 2 and 3 duplicate respectively the parametric and geometric soundings illustrated in PODDAR [1983]. The same models were used to compute H_r in parallel with H_z, and are also plotted in Figures 2 and 3.

PODDAR [1983] compared his results with RYU et al. [1970], where the latter authors used a circular loop source. As shown in *Figure 2*, the FHT method agrees quite well with the results from PODDAR [1983, Fig. 2] and RYU et al. [1970]. The amplitude scale in Figure 2 is unnormalized (Amps/m.) as in Poddar's Figure 2; however, a normalized mutual coupling ratio H/Z_0 was used in *Figure 3*, instead of amplitude given in dB as in Poddar's Figure 3. The normalization factor Z_0 is defined as the free space field from a rectangular loop source of current and is given by PODDAR [1982, p. 104]. The H_z/Z_0 mutual coupling ratio amplitude in Figure 3 approaches unity for all soundings near the loop for $X \geq 200$; and as expected, the H_r/Z_0 amplitude approaches zero near the loop center for all H_r soundings.

The behavior of the H_r and H_z fields outside the rectangular loop for the same model as in Figure 3 is depicted in *Figure 4*. Figure 4 shows the normalized H_r and H_z field geometric soundings for $Y=0$ and $X \geq 300$. Note that the amplitude of H_z/Z_0 approaches unity near the source (as in Figure 3), but depending on the layer thicknesses, it can either increase or decrease from unity as X increases. The behavior of H_r/Z_0 similarly approaches zero on either side of the nearest rectangle leg. The field components are continuous as the source is approached by (X, Y), but nevertheless, they cannot be evaluated accurately at extremely small r values.

The field components in the first quadrant outside the loop, near the corner point (250, 250), are illustrated in *Figure 5*, where $Y=275$ and $X \geq 0$ were used in the geometric soundings. The flat responses for $0 \leq X < 250$ in both amplitude and phase spectra are due almost entirely to the nearest rectangular leg. For $X > 250$, all four legs begin to contribute more to the total field at larger r distances.

As a final example of parametric soundings, the model in Figure 2 was used with two different layer thicknesses, and computed at the observation point (2, 3), wich was specifically offset from (0, 0) so that H_r was non-zero. The results are given in *Figure 6*.

The unnormalized amplitude shapes for H_r and H_z in Figures 2 and 6 are somewhat similar; however, a noticeable phase jump from -180 to $+180$ degrees occurs for H_r inside but not outside the loop (compare Figures 2d and 6d). This is an artifact of representing phase angles in the range $(-180, 180)$ degrees instead of (0, 360) degrees. A choice was made so that the phase angles of H_z and H_z/Z_0 were in the same quadrants inside or outside the loop, whereas the phase angles of H_r or H_r/Z_0 differed by 180 degrees inside and outside. Thus the phase angles of the unnormalized fields and normalized fields are identical and in the same quadrants for points outside the loop, but are 180 degrees out-of-phase for points inside the loop. Regardless of how phase angles are

defined for normalized or unnormalized fields, this could lead to difficulty, for example, in joint inversion of phase data taken both inside and outside a rectangular loop. Of course, the use of real and quadrature soundings (instead of amplitude and phase) would alleviate this cumbersome situation.

Fig. 2. Parametric soundings outside a square loop ($a = b = 10$ m) at a distance of $Y = 100$ m from the loop center, and computed over a given induction number ($B = R_0/\delta$) range. The 2-layer model form PODDAR [1983, Fig. 2] was used, where $\sigma_1 = 0.01$ S/m, $\sigma_2 = 0.3$ S/m, and h was varied as indicated in the legends
a) Unnormalized amplitude H_z versus B,
b) phase H_z versus B,
c) unnormalized amplitude H_r versus B, and
d) phase H_r versus B

2. ábra. Paraméter szondázások a négyzetalakú hurkon kívül ($a = b = 10$ m), a hurok középpontjától $Y = 100$ m távolságra, egy adott indukció szám ($B = R_0/\delta$) tartományon számítva. PODDAR [1983, 2. ábra] 2-réteges modelljét használtuk, ahol $\sigma_1 = 0{,}01$ S/m, $\sigma_2 = 0{,}3$ S/m és h úgy változott, ahogy azt a jelmagyarázat feltünteti
a) A normálatlan H_z amplitúdó B függvényében,
b) a H_z fázis B függvényében,
c) a normálatlan H_r amplitúdó B függvényében és
d) a H_r fázis B függvényében

Рис. 2. Параметрические зондирования вне прямоуголного контура ($a = b = 10$ м) в расстоянии $Y = 100$ м от центра контура; для данного интервала чисел индукции ($B = R_0/\delta$). Использован двухслойный модель ПОДДАРА [1983, рис. 2], при которым: $\sigma_1 = 0{,}01$ сименс/м, $\sigma_2 = 0{,}3$ сименс/м. h изменяется согласно рисунку
а) ненормированная амплитуда H_z в зависимости от B,
b) фаза H_z в зависимости от B,
c) ненормированная амплитуда H_r в зависимости от B,
d) фаза H_r в зависимости от B

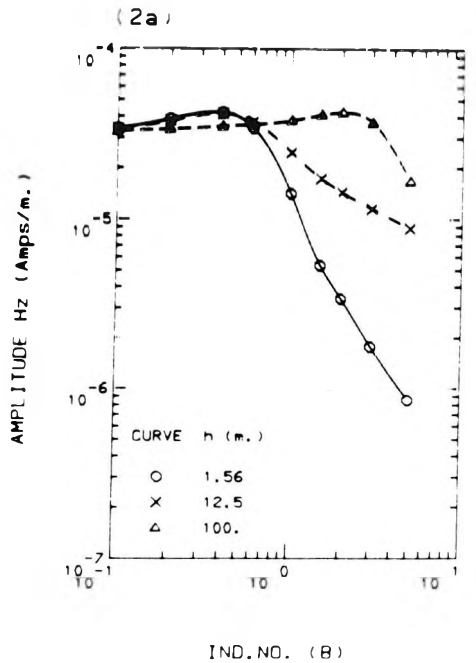
(2a)
AMPLITUDE Hz (Amps/m.)
CURVE h (m.)
1.56
12.5
100.
IND.NO. (B)

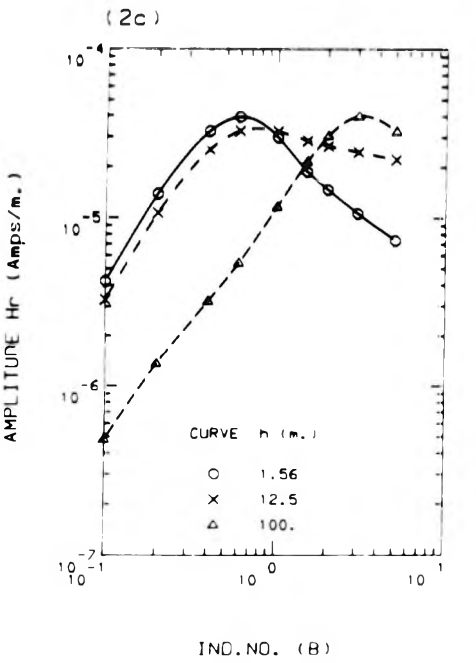
(2c)
AMPLITUDE Hr (Amps/m.)
CURVE h (m.)
1.56
12.5
100.
IND.NO. (B)

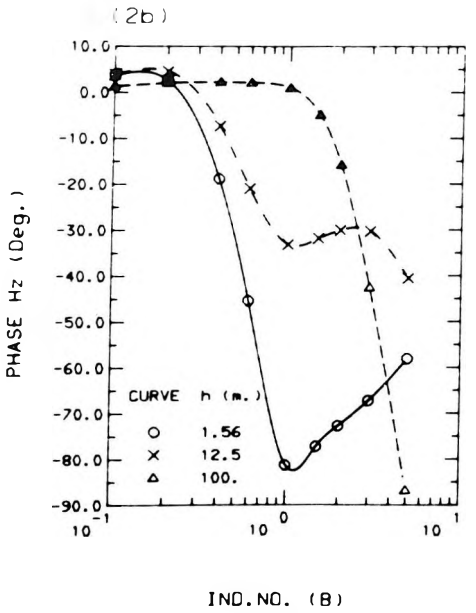
(2b)
PHASE Hz (Deg.)
CURVE h (m.)
1.56
12.5
100.
IND.NO. (B)

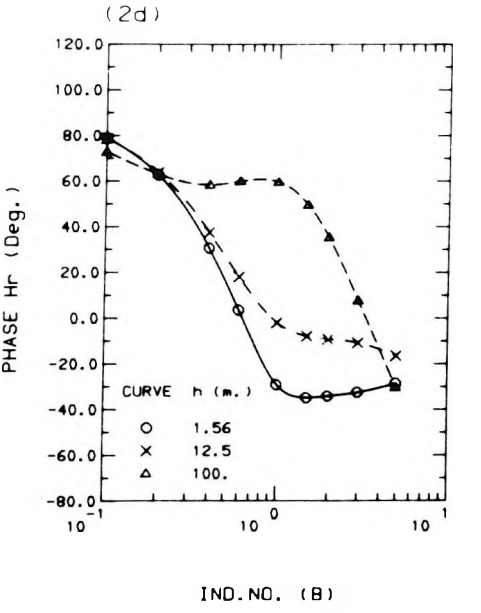
(2d)
PHASE Hr (Deg.)
CURVE h (m.)
1.56
12.5
100.
IND.NO. (B)

Fig. 3. Geometric soundings inside a square loop ($a=b=250$ m) at $Y=0$ where X was varied from 25 to 225 m in increments of 25 m. The 3-layer model from PODDAR [1983, Fig. 3] was used, where $\sigma_1=0.01$ S/m, $\sigma_2=0.03$ S/m, $\sigma_3=0.001$ S/m, $h_1=3$ m, $f=1344$ Hertz, and h_2 was varied as indicated in the legends
a) Normalized amplitude H_z/Z_0 versus X,
b) phase H_z/Z_0 versus X,
c) normalized amplitude H_r/Z_0 versus X, and
d) phase H_r/Z_0 versus X

3. ábra. Geometriai szondázás a négyzet alakú hurkon belül ($a=b=250$ m) $Y=0$-nál, X pedig 25-től 225 m-ig növekedett, 25 m-es lépésekben. PODDAR [1983, 3. ábra] 3-réteges modelljét használtuk, ahol $\sigma_1=0{,}01$ S/m, $\sigma_2=0{,}03$ S/m, $\sigma_3=0{,}001$ S/m, $h_1=3$ m, $f=1344$ Hz és h_2 úgy változott, ahogy azt a jelmagyarázat feltünteti
a) A H_z/Z_0 normált amplitúdó X függvényében,
b) a H_z/Z_0 fázis X függvényében,
c) a H_r/Z_0 normált amplitúdó X függvényében és
d) a H_r/Z_0 fázis X függvényében

Рис. 3. Дистанционное зондирование внутри контура ($a=b=250$ м), $Y=0$; X изменяется по 25 м от 25 м до 225 м. Использован трехслойный модель Поддара [1983, рис. 3], при котором $\sigma_1=0{,}01$ сименс/м, $\sigma_2=0{,}03$ сименс/м, $\sigma_3=0{,}001$ сименс/м, $h_1=3$ м, $f=1344$ Гц, h_2 изменяется согласно рисунку
а) нормированная амплитуда H_z/Z_0 в зависимости от X,
b) фаза H_z/Z_0 в зависимости от X,
c) нормированная амплитуда H_r/Z_0 в зависимости от X,
d) фаза H_r/Z_0 в зависимости от X

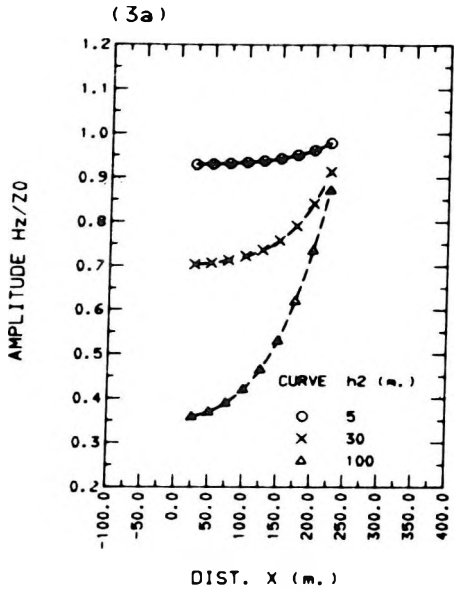
(3a)
AMPLITUDE Hz/Z0
DIST. X (m.)
CURVE h2 (m.)
5
30
100

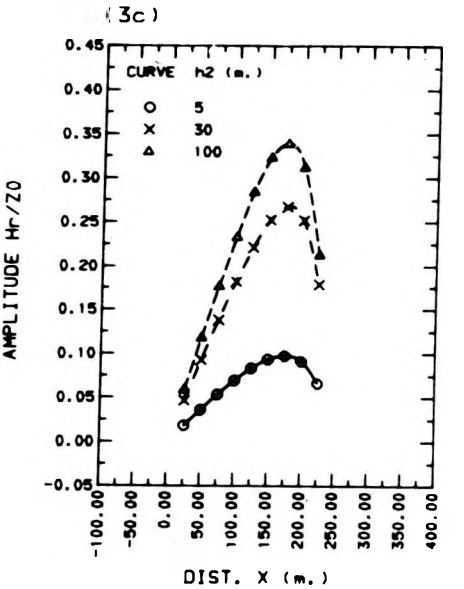
(3c)
AMPLITUDE Hr/Z0
DIST. X (m.)
CURVE h2 (m.)
5
30
100

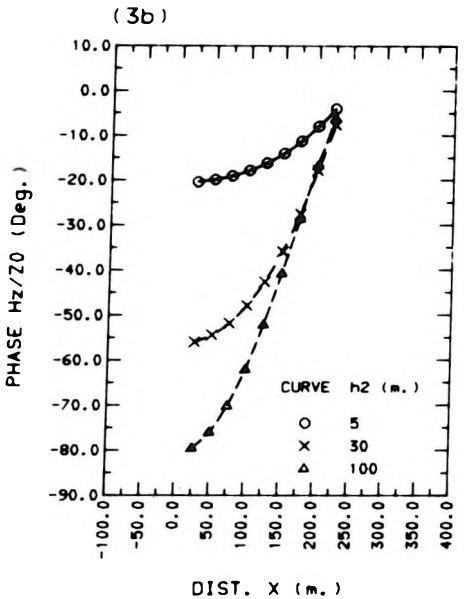
(3b)
PHASE Hz/Z0 (Deg.)
DIST. X (m.)
CURVE h2 (m.)
5
30
100

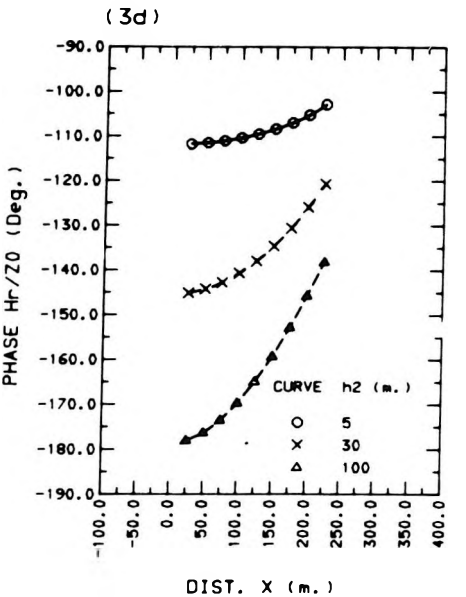
(3d)
PHASE Hr/Z0 (Deg.)
DIST. X (m.)
CURVE h2 (m.)
5
30
100

Fig. 4. Geometric soundings outside a square loop ($a=b=250$ m) at $Y=0$ where X was varied from 300 to 1000 m in increments of 100 m. The 3-layer model from PODDAR [1983, Fig. 3] was used, where $\sigma_1=0.01$ S/m, $\sigma_2=0.03$ S/m, $\sigma_3=0.001$ S/m, $h_1=3$ m, f=1344 Hertz, and h_2 was varied as indicated in the legends
a) Normalized amplitude H_z/Z_0 versus X,
b) phase H_z/Z_0 versus X,
c) normalized amplitude H_r/Z_0 versus X, and
d) phase H_r/Z_0 versus X

4. ábra. Geometriai szondázások a négyzet alakú hurkon ($a=b=250$ m) kívül $Y=0$-nál, X pedig 300 m-től 1000 m-ig változott 100 m-es lépésekben. PODDAR [983, 3. ábra] 3-réteges modelljét használtuk, ahol $\sigma_1=0{,}01$ S/m, $\sigma_2=0{,}03$ S/m, $\sigma_3=0{,}001$ S/m, $h_1=3$ m, $f=1344$ Hz és h_2 úgy változik, ahogy azt a jelmagyarázat feltünteti
a) A H_z/Z_0 normált amplitúdó X függvényében,
b) a H_z/Z_0 fázis X függvényében és
c) a H_r/Z_0 normált amplitúdó X függvényében
d) a H_r/Z_0 fázis X függvényében

Рис. 4. Дистанционные зондирования вне контура ($a=b=250$ м), $Y=0$; X изменяется по 100 м от 300 м до 1000 м. Использован трехслойный модель ПОДДАРА [1983, рис. 3], при котором $\sigma_1=0{,}01$ сименс/м, $\sigma_2=0{,}03$ сименс/м, $\sigma_3=0{,}001$ сименс/м, $h_1=3$ м, $f=1344$ Гц, h_2 изменяетсяпо по условным обозначениям
а) нормированная амплитуда H_z/Z_0 в зависимости от X,
b) фаза H_z/Z_0 в зависимости от X
c) нормированная амплитуда H_r/Z_0 в зависимости от X,
d) фаза H_r/Z_0 в зависимости от X

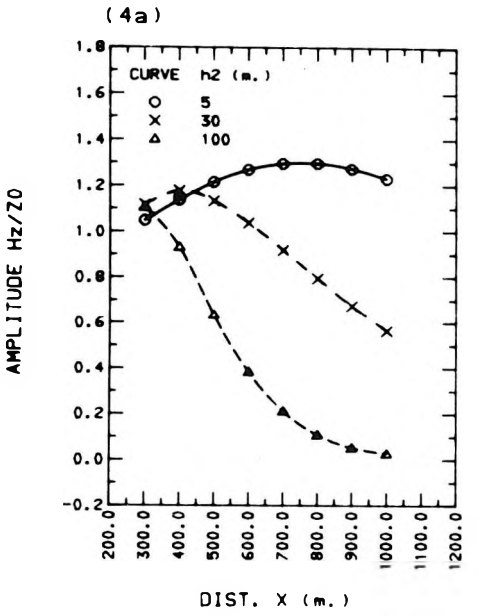
(4a)
CURVE h2 (m.)
5
30
100
AMPLITUDE Hz/Z0
DIST. X (m.)

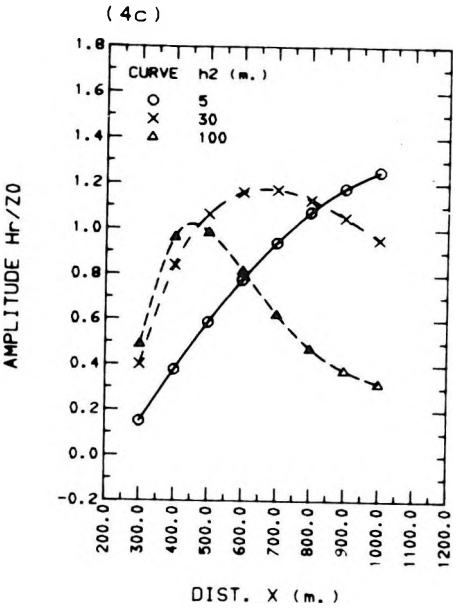
(4c)
CURVE h2 (m.)
5
30
100
AMPLITUDE Hr/Z0
DIST. X (m.)

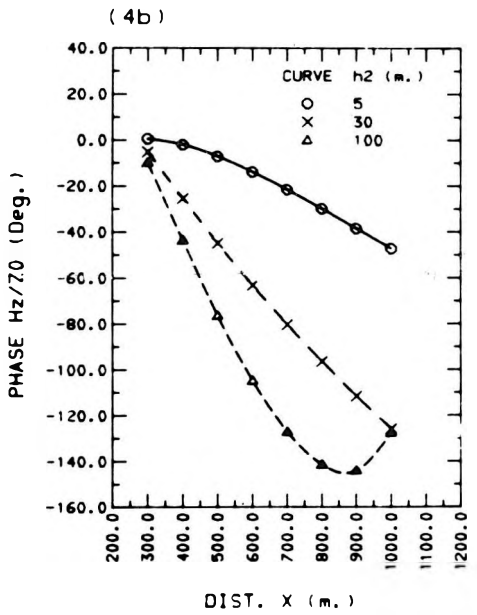
(4b)
CURVE h2 (m.)
5
30
100
PHASE Hz/Z0 (Deg.)
DIST. X (m.)

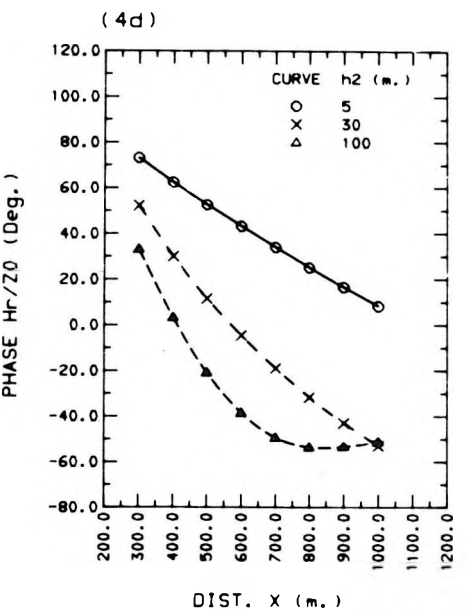
(4d)
CURVE h2 (m.)
5
30
100
PHASE Hr/Z0 (Deg.)
DIST. X (m.)

Fig. 5. Geometric soundings in quadrant I near the corner point (250,250) for a square loop ($a=b=250$ m) at $Y=275$ where X was varied from 0 to 500 m in increments of 50 m. The 3-layer model from PODDAR [1983, Fig. 3] was used, where $\sigma_1=0.01$ S/m, $\sigma_2=0.03$ S/m, $\sigma_3=0.001$ S/m, $h_1=3$ m, $f=1344$ Hertz, and h_2 was varied as indicated in the legends
a) Normalized amplitude H_z/Z_0 versus X,
b) phase H_z/Z_0 versus X,
c) normalized amplitude H_r/Z_0 versus X, and
d) phase H_r/Z_0 versus X

5. ábra. Geometriai szondázások az I. síknegyedben, a négyzet alakú hurok ($a=b=250$ m) (250,250) sarokpontjának közelében, $Y=275$-nél, X pedig 0-tól 500 m-ig változott 50 m-es lépésekben. PODDAR [1983, 3. ábra] 3-réteges modelljét használtuk, ahol $\sigma_1=0{,}01$ S/m, $\sigma_2=0{,}03$ S/m, $\sigma_3=0{,}001$ S/m, $h_1=3$ m, $f=1344$ Hz és h_2 úgy változott, ahogy azt a jelmagyarázat feltünteti
a) A H_z/Z_0 normált amplitúdó X függvényében,
b) a H_z/Z_0 fázis X függvényében,
c) a H_r/Z_0 normált amplitúdó X függvényében,
d) a H_r/Z_0 fázis X függvényében

Рис. 5. Дистанционные зондирования в первой четверти плоскости, вблизи угловой точки контура квадратной ($a=b=250$ м) формы. $Y=275$; X изменяется по 50 м от 0 до 500 м. Использован трехслойный модель ПОДДАРА [1983, рис. 3] при котором $\sigma_1=0{,}01$ сименс/м, $\sigma_2=0{,}03$ сименс/м, $\sigma_3=0{,}001$ сименс/м, $h_1=3$ м, $f=1344$ Гц, h_2 изменяется согласно условным обозначениям
а) нормированная амплитуда H_z/Z_0 в зависимости от X,
b) фаза H_z/Z_0 в зависимости от X,
c) нормированная амплитуда H_r/Z_0 в зависимости от X,
d) фаза H_r/Z_0 в зависимости от X

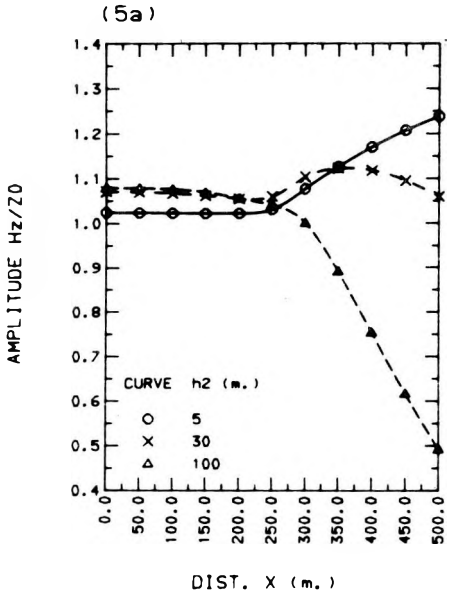
(5a)
AMPLITUDE Hz/Z0
CURVE h2 (m.)
5
30
100
DIST. X (m.)

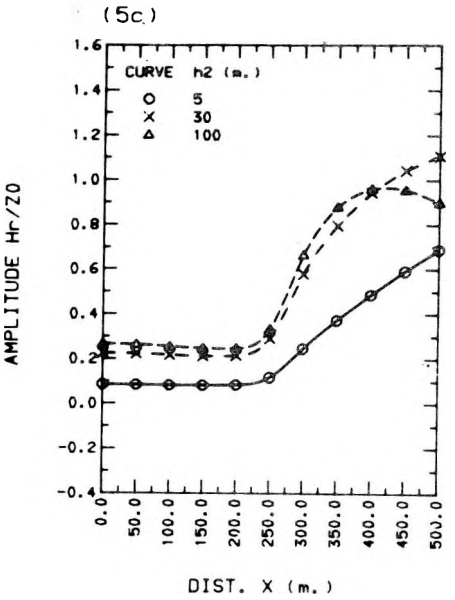
(5c)
AMPLITUDE Hr/Z0
CURVE h2 (m.)
5
30
100
DIST. X (m.)

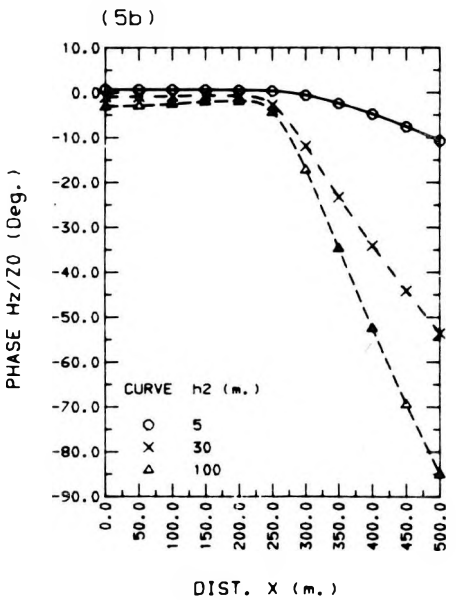
(5b)
PHASE Hz/Z0 (Deg.)
CURVE h2 (m.)
5
30
100
DIST. X (m.)

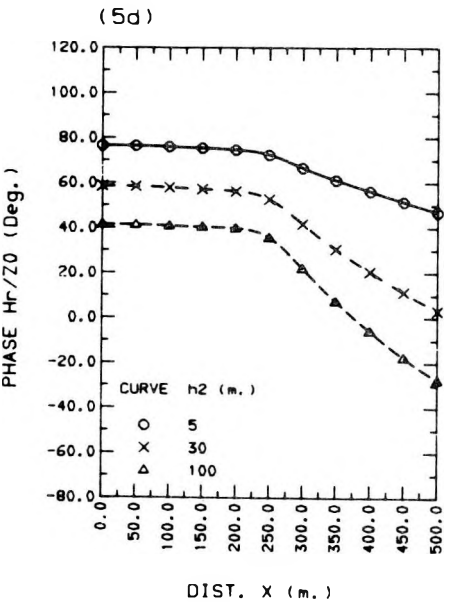
(5d)
PHASE Hr/Z0 (Deg.)
CURVE h2 (m.)
5
30
100
DIST. X (m.)

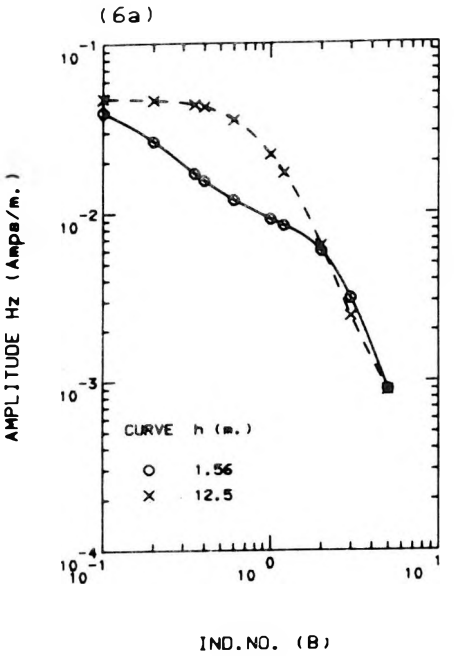
(6a)
AMPLITUDE Hz (Amps/m.)
CURVE h (m.)
1.56
12.5
IND.NO. (B)

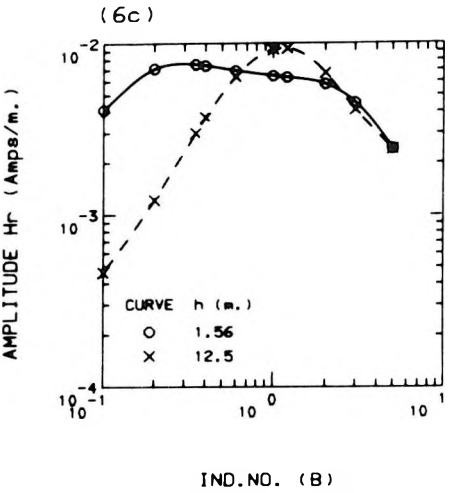
(6c)
AMPLITUDE Hr (Amps/m.)
CURVE h (m.)
1.56
12.5
IND.NO. (B)

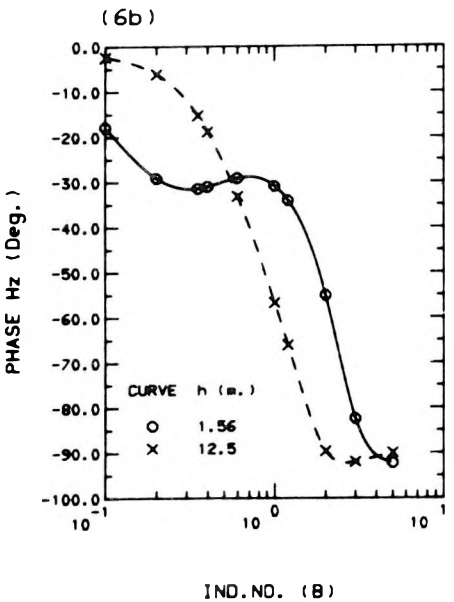
(6b)
PHASE Hz (Deg.)
CURVE h (m.)
1.56
12.5
IND.NO. (B)

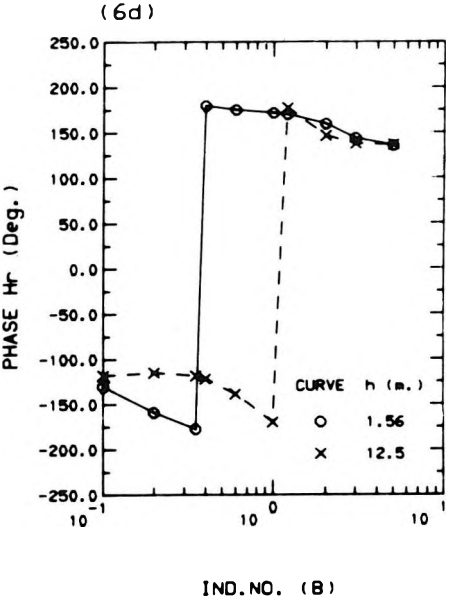
(6d)
PHASE Hr (Deg.)
CURVE h (m.)
1.56
12.5
IND.NO. (B)

Fig. 6. Parametric soundings near the loop center for a square loop ($a = b = 10$ m) at the point ($X = 2$, $Y = 3$), and computed over a given induction number ($B = R_0/\delta$) range. The 2-layer model from PODDAR [1983, Fig. 2] was used, where $\sigma_1 = 0.01$ S/m, $\sigma_2 = 0.3$ S/m, and h was varied as indicated in the legends
a) Unnormalized amplitude H_z versus B,
b) phase H_z versus B,
c) unnormalized amplitude H_r versus B, and
d) phase H_r versus B.

6. ábra. Paraméter szondázások egy négyzet alakú hurok ($a = b = 10$ m) középpontjának közelében, az ($X = 2$, $Y = 3$) pontban, egy adott indukció szám ($B = R_0/\delta$) tartományon számítva. PODDAR [1983, 2. ábra] 2-réteges modelljét használtuk, ahol $\sigma_1 = 0{,}01$ S/m, $\sigma_2 = 0{,}3$ S/m és h úgy változott, ahogy a jelmagyarázat feltünteti
a) A normálatlan H_z amplitúdó B függvényében,
b) a H_z fázis B függvényében,
c) a normálatlan H_r amplitúdó B függvényében és
d) a H_r fázis B függvényében

Рис. 6. Параметрические зондирования вблизи центра контура квадратной формы, ($a = b = 10$ м), в точке ($X = 2$, $Y = 3$), для данного интервала чисел индукции ($B = R_0/\delta$). Использован двухслойный модель ПОДДАРА [1983, рис. 2], при котором $\sigma_1 = 0{,}01$ сименс/м, $\sigma_2 = 0{,}3$ сименс/м, h изменяется согласно условным обозначениям
a) ненормированная амплитуда H_z в зависимости от B,
b) фаза H_z в зависимости от B,
c) ненормированная амплитуда H_r в зависимости от B,
d) фаза H_r в зависимости от B

5. Conclusions

A new algorithm was discussed that evaluates simultaneously the radial H_r and vertical H_z magnetic fields inside or outside a rectangular loop source of current on a multilayered earth. A fast Hankel transform algorithm [ANDERSON 1982] is the basis for the new solution, which in turn, reduces the overall computation of either H_r or H_z to four elementary spline-function integrations. Accuracy of this method is at least comparable to that obtained with dipole or circular loop source methods. Because of the improved speed of the calculations, future uses of this technique during inverse solutions in either frequency- or time-domains would be nearly as practical for rectangular loops as for dipole sources. The general idea presented can be readily extended to additionally compute the electric field components about a rectangular loop source. Further extensions and savings could be realized by storing intermediate FHT results for repetitive calculations using the same earth model while varying the loop size and/or position.

REFERENCES

ALBERG J. H., NILSON E. N., and WALSH J. L. 1967: The theory of splines and their applications. Academic Press, New York, 284 p.

ANDERSON W. L. 1979: Numerical integration of related Hankel transforms of orders 0 and 1 by adaptive digital filtering. Geophysics, **44,** 7, pp. 1287–1305

ANDERSON W. L. 1982: Fast Hankel transforms using related and lagged convolutions. Association for Computing Machinery Transactions on Mathematical Software, **8,** 4, pp. 344–368

ANDERSON W. L. 1984: Fast evaluation of Hr and Hz field soundings near a rectangular loop source on a layered earth (Program HRZRECT). U.S. Geological Survey Open-File Report 84–257, 80 p.

ANDERSON W. L. 1985: Computation of transient soundings for the time-derivative of Hz near a rectangular loop source on a layered earth (Program FWDTHZ). U.S. Geological Survey Open-File Report 85–270, 44 p.

BOERNER D. E., and WEST G. F. 1984: Efficient calculation of the electromagnetic fields of an extended source. Geophysics, **49,** 11, pp. 2057–2060

FRISCHKNECHT F. C. 1967: Fields about an oscillating magnetic dipole over a two-layer earth and application to ground and electromagnetic surveys. Quarterly of the Colorado School of Mines, **62,** 1, 326 p.

KAUAHIKAUA J. 1978: Electromagnetic fields about a horizontal electric wire source of arbitrary length. Geophysics, **43,** 5, pp. 1019–1022

KRISTENSSON G. 1983: The electromagnetic field in a layered earth induced by an arbitrary stationary current distribution. Radio Science, **18,** 3, pp. 357–368

PATTERSON T. N. L. 1973: Algorithm for automatic numerical integration over a finite interval. Comm. of the ACM, **16,** 11, pp. 694–699

PODDAR M. 1982: A rectangular loop source of current on a two-layered earth. Geophysical Prospecting, **30,** 1, pp. 101–114

PODDAR M. 1983: A rectangular loop source of current on multilayered earth. Geophysics, **48,** 1, pp. 107–109

RYU J., MORRISON H. F., and WARD S. H. 1970: Electromagnetic fields about a loop source of current. Geophysics, **35,** 5, pp. 862–896

WAIT J. R. 1958: Induction by an oscillating dipole over a two-layer ground. Appl. Sci. Res., v. B–7, pp. 73–80

WAIT J. R. 1966: Fields of a horizontal dipole over a stratified anisotropic half-space. IEEE Trans. on Antennas and Propagation, **AP–14,** 6, pp. 790–792

A RADIÁLIS ÉS FÜGGŐLEGES MÁGNESES TÉR GYORS SZÁMÍTÁSA RÉTEGZETT FÖLDÖN FEKVŐ, TÉGLALAP ALAKÚ HUROKFORRÁS KÖZELÉBEN

Walter L. ANDERSON

Gyors Hankel-transzformációs (FHT) algoritmust alkalmaz a rétegzett föld felszínén fekvő, téglalap alakú hurokforráson belüli vagy azon kívüli, radiális vagy függőleges mágneses tér felhasználásával végzett paraméter (vagy geometriai) szondázások görbéinek egyidejű számítására. Az FHT a lineáris digitális szűrés elvét használja fel és ha a téglalap alakú hurok problémájára alkalmazzuk, minden egyes térszámítás négy elemi spline integrálásra egyszerűsödik. Paraméter szondázás esetén az FHT-re csak egyszer van szükség minden egyes frekvencián; geometriai szondázás esetén az FHT-t csak egyszer kell végrehajtani ahhoz, hogy megkapjuk mindkét térösszetevőt. Az FHT módszernek a meglévő, dipólra, köralakú és téglalap alakú hurokra vonatkozó egyenes feladat megoldásokkal való összehasonlítása azt mutatja, hogy legalább három számjegyes pontosság érhető el jelentősen csökkentett számítási idő mellett is. Ennek következtében az inverz feladat megoldása mind a frekvencia-, mind az időtartományban gyakorlatilag is lehetséges lesz téglalap alakú hurokforrása éppúgy, mint dipólforrásra.

БЫСТРОЕ ВЫЧИСЛЕНИЕ РАДИАЛЬНОГО И ВЕРТИКАЛЬНОГО МАГНИТНОГО ПОЛЯ ВБЛИЗИ ВОЗБУЖДАЮЩЕЙ ПЕТЛИ ПРЯМОУГОЛНОЙ ФОРМЫ, НАХОДЯЩЕЙСЯ НА ПОВЕРХНОСТИ СЛОИСТОЙ СРЕДЫ

Вальтер Л. АНДЕРСОН

Применяется алгоритм быстрой Хенкел-трансформации (FHT) для вычисления кривых зондирований (параметрических или дистанционных), проведенных с применением радиальных или вертикальных компонентов магнитного поля прямоугольного контура, находящегося на поверхности слоистой среды. При FHT используется принцип линейной цифровой фильтрации. В случае прямоугольного контура вычисления полей превращается в интеграцию четырех элементарных «сплайнов». При параметрическом зондировании нужен FHT только раз на каждую частоту. При геометрическом зондировании для вычисления обоих компонентов нужен FHT только один раз. Сопоставление результатов, полученных с применением FHT с результатами существующих решений прямых задач для диполя и петлей круглой и прямоугольной форм указывает на то, что достигается точность порядка трех цифров, существенно сокращая и время вычислений. Благодаря этого практически можно решать и обратные задачи для прямоугольного контура и для диполя так в частотных, как и временных диапазонах.

GEOPHYSICAL TRANSACTIONS 1985
Vol. 31. No. 4. pp. 359–371

CALCULATING GALVANIC ANOMALIES FOR AN INCLINED PRISM IN A TWO-LAYERED HALF-SPACE

Heikki SOININEN*

The current paper presents a computation program applicable to the numerical modelling of apparent resistivity and induced polarization anomalies. The field problem is solved using the integral equation technique. The elementary model in the program package is an inclined prism in a two-layered half-space. All the resistivities describing media can be complex and dispersive, and hence modelling of the wide-band induced polarization method is possible. The values of dispersive resistivity can either be inserted in the program from petrophysical measurements directly or the frequency behaviour can be described with the aid of a mathematical dispersion model.

The behaviour of anomalies obtained with the gradient array and the dipole–dipole array are compared using various geological structural models. The dipole–dipole array is better than the gradient one for locating a thin, vertical body because the anomaly to be measured thereby is greater, but then again, the dip is considerably easier to interpret with the gradient array than with the dipole–dipole one.

In the case of a large target, the induced polarization anomaly measured with the gradient array is attenuated very slowly with increasing depth to the upper surface of the conductive body (in short: depth to the upper surface). Hence, the gradient array is more effective than the dipole–dipole array in the search for large bodies but the dipole–dipole array is more suitable than the gradient array in determination of the depth to the upper surface.

A conductive overburden substantially attenuates the response of galvanic methods measured on the surface of the earth because a large part of the current is channelled to pass through the overburden.

Keywords: numerical modelling, galvanic methods, apparent resistivity, induced polarization, integral equations

1. Introduction

In the numerical modelling of galvanic methods the integral equation technique has been used in the case of a $2\frac{1}{2}$-dimensional model, arbitrary in cross-section, located in a homogeneous half-space [ESKOLA and HONGISTO 1981] and in the case of a three-dimensional rectangular prism model [ESKOLA 1979]. In these, the problem was formulated as a Fredholm integral equation of the second kind for the electric field. ELORANTA [1984] has presented a method for calculating the apparent resistivity and mise-à-la-masse anomalies of good conductors located in a homogeneous half-space. The conductive bodies are considered as equipotential domains. The problem has been formulated as a Fredholm integral equation of the first kind.

* Geological Survey of Finland, SF–02150 Espoo 15, Finland
Manuscript received (revised form): 22 February, 1985

The present work describes a method of calculating galvanic anomalies in which the solution of the field problem is formulated as by ESKOLA [1979] with a Fredholm integral equation of the second kind. The applicability of the method presented by Eskola has been expanded so that the elementary model in the program is an inclined prism in a two-layered half-space. All the resistivities of the model can be complex and dispersive, so that it is possible with the program to compute wide-band induced polarization (IP) model anomalies of phase-angle and amplitude spectra [SOININEN 1984, 1985]. The dispersive resistivities required as input data can be taken from petrophysical laboratory or in-situ determinations directly. It is also possible to use dispersion models [PELTON et al. 1983], such as the Cole-Cole model, which describe the frequency behaviour of the resistivity.

The program can be applied not only to the IP method but also to the three-dimensional modelling of resistivity profiling and sounding.

2. The integral equation

Let us examine media that are homogeneous, linear and isotropic in electric conductivity. Let S be the boundary surface between two domains containing different media. The conductivities of the domains are σ_e and σ_b. The field problem of the static current system can be presented on boundary surface S by means of the Fredholm integral equation of the second kind written for the normal component of the electric field as follows [ESKOLA 1979]:

$$E_n(\bar{r}) = E_{on}(\bar{r}) + \int_S Q G_n(\bar{r}|\bar{r}_o) E_n(\bar{r}_o) ds_o , \tag{1}$$

where E_n is the normal component of the electric field on the discontinuity surface S of conductivity on side e of material; E_{on} is the normal component of the primary field; G_n is Green's function of the normal component of the electric field for the basic structure used; r is the calculation point; r_o is the source point; and

$$Q = (1/4\pi\varepsilon_o)\frac{(\sigma_e/\sigma_b)-1}{(1/\varepsilon_o)-j\omega/\sigma_b},$$

where ω is the angular frequency, ε_o is the dielectric permittivity of free space, and $j^2 = -1$. Because, usually, $1/\varepsilon_o >> |\omega/\sigma_b|$ we can approximate, thus:

$$Q = (1/4\pi)(\sigma_e/\sigma_b - 1).$$

The integration area S contains all the boundary surfaces of domains differing in conductivity contrast.

Equation (1) can be solved numerically by dividing boundary surface S into elements s_i and postulating that equation (1) holds at the centre of each element (i) and by presuming further that the normal component of the electric field is constant in each element. Thus we obtain the linear set of equations:

$$E_n(i) = E_{on}(i) + \sum_k Q\bar{G}_n(i|k)\, E_n(k) \text{ for each element } (i), \tag{2}$$

where $\bar{G}_n$ is the Green function of the normal component of the electric field of the source element, i refers to the computation element and k to the source element. The case in which the computation point is located in the source element ($i=k$) need not be treated separately because integrated Green's functions $\bar{G}_n$ are not singular.

In the program presented, the linear set of equations (2) is solved using Gaussian elimination. As a result we obtain the normal components of the electric field at the centres of the elements. Finally the potential Φ or required component E_p of the electric field can be calculated for the computation point from the equations:

$$\Phi(\bar{r}) = \Phi_o(\bar{r}) + \sum_k Q\bar{G}(\bar{r}|k)E_n(k) \quad \text{and} \tag{3}$$

$$E_p(\bar{r}) = E_{op}(\bar{r}) + \sum_k Q\bar{G}_p(\bar{r}|k)E_n(k), \tag{4}$$

where Φ_o is the primary potential; E_{op} is the p component of the primary field; and $\bar{G}$ is Green's function of the potential of the source element; and $\bar{G}_p$ is the corresponding Green's function of the p component of the electric field.

2.1 Green's functions of the source elements

In the program implemented, the elementary model is an inclined prism whose upper and lower faces are perpendicular to the z-axis. The basic structure is a two-layered half-space *(Figure 1)*. In the numerical solution the faces are divided into elements with segments parallel to the edges of the face. Green's functions $\bar{G}^{lj}$ of the potential of the source element and corresponding Green's functions $\bar{G}_p^{lj}$ of the p component of the electric field can be obtained by integrating over the surface of the element (calculation point in layer l, source point in layer j):

$$\bar{G}^{lj}(\bar{r} \mid k) = \int_{s_k} F_{lj}\, ds_o \quad \text{and} \tag{5}$$

$$\bar{G}_p^{lj}(\bar{r} \mid k) = -\frac{\partial}{\partial p} \int_{s_k} F_{lj}\, ds_o. \tag{6}$$

The integrand F_{lj} depends on the layer in which the calculation point and the source point are located. For example, when both the calculation point and the source point are in layer 2 then with the symbols in Figure 1 [VAN NOSTRAND and COOK 1966 pp. 134–135]:

$$F_{22} = \frac{1}{R} + K \sum_{n=0}^{\infty} \frac{(-K)^n}{\sqrt{(2b(n-1)+z_0+z)^2+s^2}} + \sum_{n=0}^{\infty} \frac{(-K)^n}{\sqrt{(2nb+z_0+z)^2+s^2}}, \tag{7}$$

where

$$s^2 = (x-x_0)^2+(y-y_0)^2,$$
$$R^2 = (x-x_0)^2+(y-y_0)^2+(z-z_0)^2 \quad \text{and}$$
$$K = \frac{\varrho_1-\varrho_2}{\varrho_1+\varrho_2}, \quad (\varrho = 1/\sigma).$$

We can obtain the other functions F_{lj} in a similar fashion. Green's functions $\bar{G}^{lj}$ (integrals (5), except faces perpendicular to the y-axis) and $\bar{G}_p^{lj}$ (integrals (6)) are integrated analytically using standard integrals [GRADSHTEYN and RYZHIK 1965]. Green's functions $\bar{G}^{lj}$ of the potential of faces perpendicular to y-axis are integrated numerically.

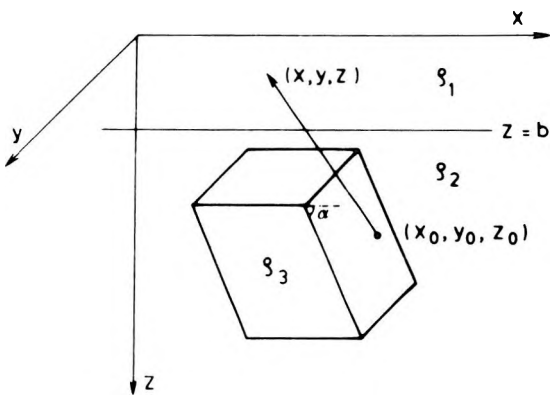

Fig. 1. Inclined prism in a two-layered half-space. The symbols used

1. ábra. Dölt prizma kétréteges féltérben

Рис. 1. Наклонная призма в двухслойной среде

2.2 Primary potential and primary field intensity

When the current electrode is in layer j and the calculation point is in layer *l* the primary potential and the *p* component of the primary electric field of a point-like current electrode are:

$$\Phi_0^{lj} = \frac{I}{4\pi\sigma_j} F_{lj} \quad \text{and} \tag{8}$$

$$E_{0p}^{lj} = -\frac{I}{4\pi\sigma_j} \frac{\partial}{\partial p} F_{lj}, \tag{9}$$

where *I* stands for the intensity of the primary current. The primary potential or the primary field required for the other current electrode configurations are obtained by summing (or integrating) the potential or the field of the point electrode.

3. Applications

The numerical solution was tested by comparing it with the results calculated using other methods. The resistivity profile was calculated for the three-dimensional prism model in *Figure 2* for a gradient array in which the distance between current electrodes is AB = 2000 m. The ratio (conductivity contrast) of the resistivity of the environment to that of the prism is 1000. Because of the large conductivity contrast it was possible to compare the result with that calculated with a program presented by ELORANTA [1984] that assumes equipotentiality. The solid line in *Figure 3/a* depicts the anomaly profile computed with the program described in the present study; the crosses depict the profile calculated with ELORANTA's [1984] program. We see that within the limits of drawing accuracy the results are identical.

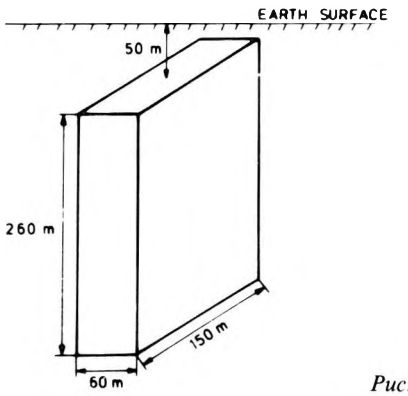

Fig. 2. Prism in an unpolarizable half-space

2. ábra. Prizma nem-gerjeszethető féltérben

Рис. 2. Призма в неполяризующемся полупространстве

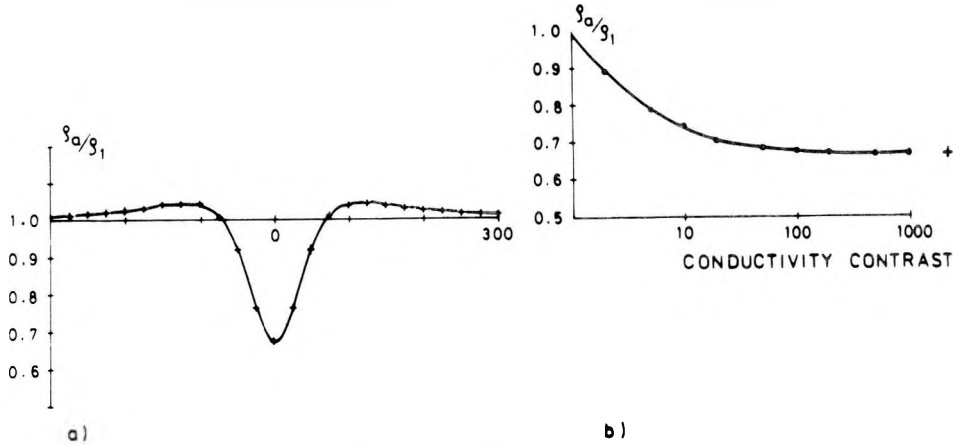

Fig. 3. a) Comparison of apparent resistivity profile computed with the present program (solid line) with the apparent resistivity profile computed with Eloranta's program (crosses)
b) Magnitude of the apparent resistivity anomaly minimum with an increase in the conductivity of the prism

3. ábra. a) Az itt bemutatott programmal számított (folytonos vonal) és Eloranta programjával számított (keresztek) látszólagos ellenállásszelvény összehasonlítása
b) A látszólagos ellenállás anomália minimumának változása a prizma vezetőképességének növekedésével.

Рис. 3. a) Сопоставление кривых кажущегося удельного сопротивления, вычисленного представленной программой (сплошная линия) с графиком, вычисленным программой Элоранта (крестики)
b) Изменение минимума кажущегося удельного сопротивления с увеличением проводимости призмы

To examine the development of the saturation state, the anomaly profiles were calculated for the same model with different values of conductivity contrast by increasing the conductivity of the prism. The resistivity minimum has been drawn in *Figure 3/b* as a function of conductivity contrast. We see that, for the gradient array, there is barely any change in the value of anomaly minimum when the conductivity contrast exceeds 100. This saturation effect manifests itself in equation (1) in such a way that as the conductivity contrast increases the coefficient $Q \to -1/4\pi$. Physically, saturation means that the distribution of the surface charge forming on the surface of the body changes but little as the conductivity contrast increases. The conductivity contrast at which the saturation point is reached depends on the structural model and measuring configuration used. The model calculations performed indicate that with the dipole–dipole array using various dipole separations (different values of N) we attain a somewhat wider range of conductivity contrast and that, thanks to the slower saturation, we obtain IP anomalies in a broader range of conductivity contrast than when using the gradient array.

Figure 4 shows the apparent resistivity profile and the phase-angle anomaly profile calculated for the prism model of Figure 2 and the gradient array at

frequencies f = 0.001 Hz, 0.01 Hz, 1.0 Hz and 10 Hz. The resistivity of the prism has been described by means of the Cole–Cole dispersion model [PELTON et al. 1983]:

$$Z(\omega) = R_0\left[1 - m\left(1 - \frac{1}{1 + (j\omega\tau)^c}\right)\right], \tag{7}$$

where $Z(\omega)$ = the complex impedance,
R_0 = the value of $Z(\omega)$ at zero frequency,
m = the chargeability,
c = the frequency dependence,
τ = the time constant,
ω = the angular frequency and
j^2 = -1.

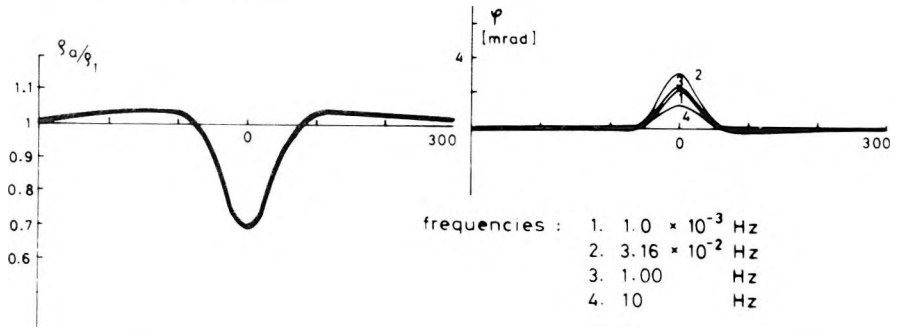

Fig. 4. Apparent resistivity profile and phase-angle anomaly profile for gradient array. AB = 2000 m. The resistivity of the prism is described with the Cole–Cole dispersion model. R_0 = 500 Ωm, m = 0.63, c = 0.32 and τ = 6.4 s. Conductivity contrast at direct current is 20

4. ábra. A gradiens elrendezéssel kapott látszólagos ellenállás- és fázis szelvény. AB = 2000 m. A prizma ellenállását a Cole–Cole diszperziós modell írja le. R_0 = 500 Ωm, m = 0,63, c = 0,32 és τ = 6,4 s. Az egyenáramra vonatkozó vezetőképesség kontraszt 20

Рис. 4. Графики кажущегося сопротивления и фазы, полученных градиентной установкой. AB = 2000 м. Сопротивление призмы описывается дисперсионным моделем Кол–Кол. R_0 = 500 Ωм, m = 0,63, c = 0,32 и τ = 6,4 сек. Контраст по сопротивлению для постоянного тока является 20-тикратным

The parameters are R_0 = 500 Ωm, m = 0.63, c = 0.32 and τ = 6.4 s. The resistivity of the environment is (real) ϱ_2 = 10,000 Ωm, and hence the conductivity contrast at direct current is 20. *Figure 5* depicts corresponding profiles for the dipole–dipole array (a = 50 m, N = 4, Na is the distance between the centres of the respective electrode pairs). We see that for a thin, vertical slab-like body the IP anomaly is substantially stronger with the dipole–dipole array than with the gradient array. In field surveys the anomaly given by the gradient array would easily escape detection because of the noise. The reason for the weak response to a thin, vertical slab by the gradient array is that, because of the

homogeneous horizontal primary field, surface charge distributions with equal absolute values but opposite in sign form on the large faces of the slab. The horizontal component of the electric field produced by these adjacent surface charges of opposite sign is small on the surface of the earth.

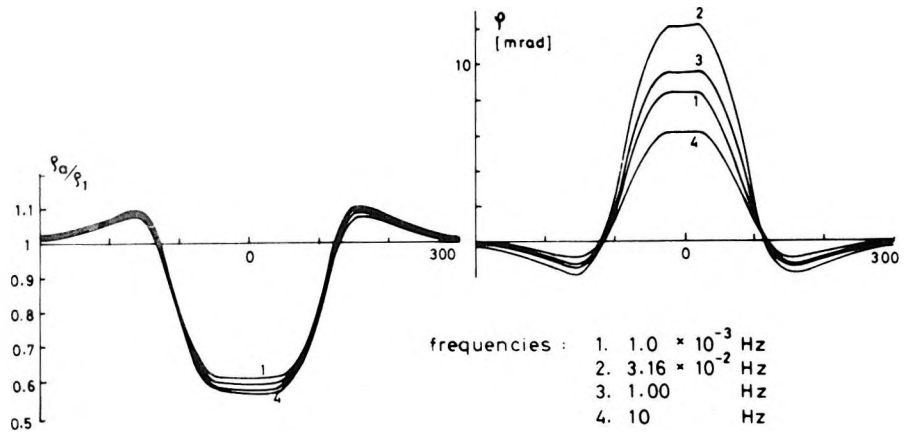

Fig. 5. Apparent resistivity profile and phase-angle anomaly profile for dipole–dipole array. $N=4$, $a=50$ m. The resitivity of the prism is described with the Cole–Cole dispersion model. $R_0=500$ Ωm, $m=0.63$, $c=0.32$ and $\tau=6.4$ s. Conductivity contrast at direct current is 20

5. ábra. A dipól–dipól elrendezéssel kapott látszólagos ellenállás- és fázis szelvény. $N=4$, $a=50$ m. A prizma ellenállását a Cole–Cole diszperziós modell írja le. $R_0=500$ Ωm, $m=0{,}63$, $c=0{,}32$ és $\tau=6{,}4$ s. Az egyenáramra vonatkozó vezetőképesség kontraszt 20

Рис. 5. Графики кажущегося сопротивления и фазы, полученных диполь–диполь установкой. $N=4$, $a=50$ м. Сопротивление призмы описывается дисперсионным моделем Кол–Кол. $R_0=500$ Ωм; $m=0{,}63$; $c=0{,}32$; $\tau=6{,}4$ сек. Контраст по сопротивлению для постоянного тока является 20-тикратным

Next the feasibilty of interpreting the dip of a slab-like body with different arrays was studied. The prism in Figure 2 dips at $\alpha = 45°$, 75° and 90°. The resistivity of the half-space is $\varrho_2 = 5000$ Ωm and the resistivity of the prism is $\varrho_3 = 25$ Ωm. *Figure 6/a* shows the calculated anomaly profiles of the apparent resistivity for gradient array at various dip angles. *Figure 6/b* depicts the corresponding profiles for the dipole–dipole array. We see that the dip has a clear effect on the gradient array anomaly and that it would be easy to interpret it qualitatively from measuring results. In contrast, the dipole–dipole array is very insensitive to dip and it is doubtful if it could be interpreted from the measuring results.

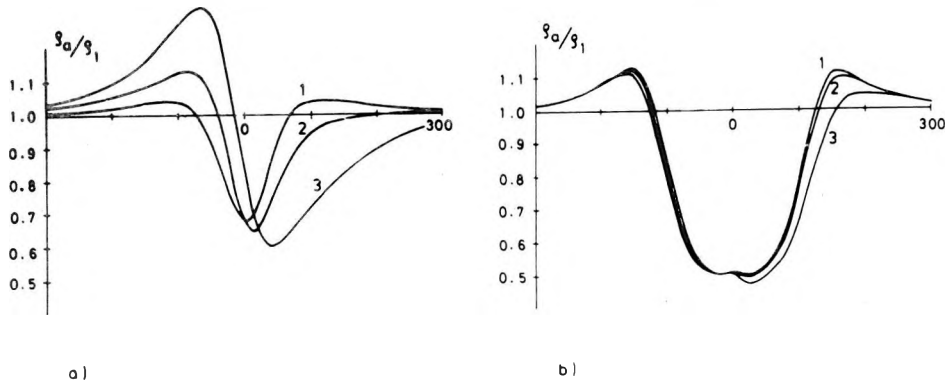

Fig. 6. Effect of dip on apparent resistivity anomaly. (1) $\alpha = 90°$, (2) $\alpha = 75°$, and (3) $\alpha = 45°$. $\varrho_2 = 5000$ Ωm, and $\varrho_3 = 25$ Ωm
a) gradient array
b) dipole–dipole array

6. ábra. A dőlés hatása a látszólagos ellenállás anomáliára. (1) $\alpha = 90°$, (2) $\alpha = 75°$ és (3) $\alpha = 45°$. $\varrho_2 = 5000$ Ωm és $\varrho_3 = 25$ Ωm
a) gradiens elrendezés
b) dipól–dipól elrendezés

Рис. 6. Влияние падения на аномалию кажущегося сопротивления. (1) $\alpha = 90°$, (2) $\alpha = 75°$, (3) $\alpha = 45°$, $\varrho_2 = 5000$ Ωм и $\varrho_3 = 25$ Ωм
a) градиентная установка
b) диполь–диполь установка

Figure 7/a shows the anomaly profiles of the apparent resistivity of the prism model of Figure 2 for gradient array. Curve 1 with conductive overburden included and curve 2 without overburden. The thickness of the overburden *(b)* is 25 m and its resistivity is $\varrho_1 = 500$ Ωm. The resistivity of the environment is $\varrho_2 = 5000$ Ωm and the resistivity of the prism is $\varrho_3 = 25$ Ωm. *Figure 7/b* shows the same profiles with dipole–dipole array ($N = 4$, $a = 50$ m). We see that the conductive overburden causes a marked reduction in the anomalies for both configurations. The conductive overburden tends to short-circuit the current, with the consequence that the bulk of the current passes through it.

Let us finally examine the attenuation of the IP anomaly caused by a large body at increasing depth to the upper surface. The IP phase-angle anomalies were calculated for the model in *Figure 8* (cube, 800 m × 800 m × 800 m) for the gradient array and for the dipole–dipole array with different values of N ($a = 20$ m). The values of resistivity for the model were taken from laboratory determinations performed on drill core samples of a polarizable gabbro massif. The magnitude of the IP phase anomaly is shown in *Figure 8* as a function of the depth to the upper surface. We see that, with the dipole–dipole array, anomalies calculated with different values of N are attenuated rapidly with increasing depth

to the upper surface whereas with the gradient array the anomalies attenuated slowly. This means in practice that a deep body, no matter how big, is hard to detect with dipole–dipole measurements because it is difficult to use sufficiently large dipole separations owing to the high transmitter output required. With the gradient array it is possible to localize a target, even at depth, but it is difficult to interpret the depth to the upper surface from the survey data.

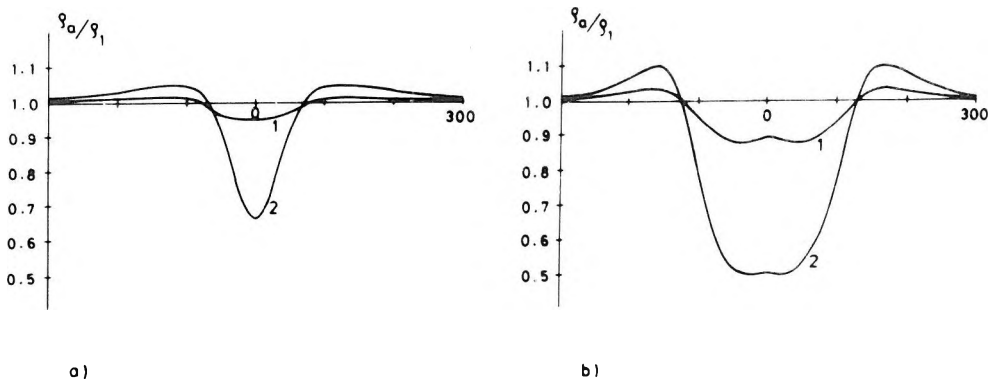

Fig. 7. Apparent resistivity profiles (1) with conductive overburden and (2) without overburden. $b = 25$ m, $\varrho_1 = 500$ Ωm, $\varrho_2 = 5000$ Ωm, and $\varrho_3 = 25$ Ωm
a) gradient array
b) dipole–dipole array

7. ábra. Látszólagos ellenállás szelvény (1) jól vezető fedő esetén és (2) fedő nélkül. $b = 25$ m, $\varrho_1 = 500$ Ωm, $\varrho_2 = 5000$ Ωm és $\varrho_3 = 25$ Ωm
a) gradiens elrendezés
b) dipól–dipól elrendezés

Рис. 7. Графики кажущегося сопротивления, (1) при покрывающем слое с большой проводимостью, (2) без покрывающего слоя. $b = 25$ м, $\varrho_1 = 500$ Ωм, $\varrho_2 = 5000$ Ωм, $\varrho_3 = 25$ Ωм
а) градиентная установка
b) диполь–диполь установка

4. Summary

The present work describes an implemented computational program package intended for the three-dimensional modelling of galvanic anomalies. The program package is in Fortran and it has been programmed for the VAX 11/780 computer at the Geological Survey of Finland. The model can be either one or more inclined prisms in a two-layered half-space. The dispersive resistivities required in IP computation can either be inserted in the program as such from the petrophysical measurements or the frequency behaviour of the resistivity can be described in the program with the aid of a dispersion model.

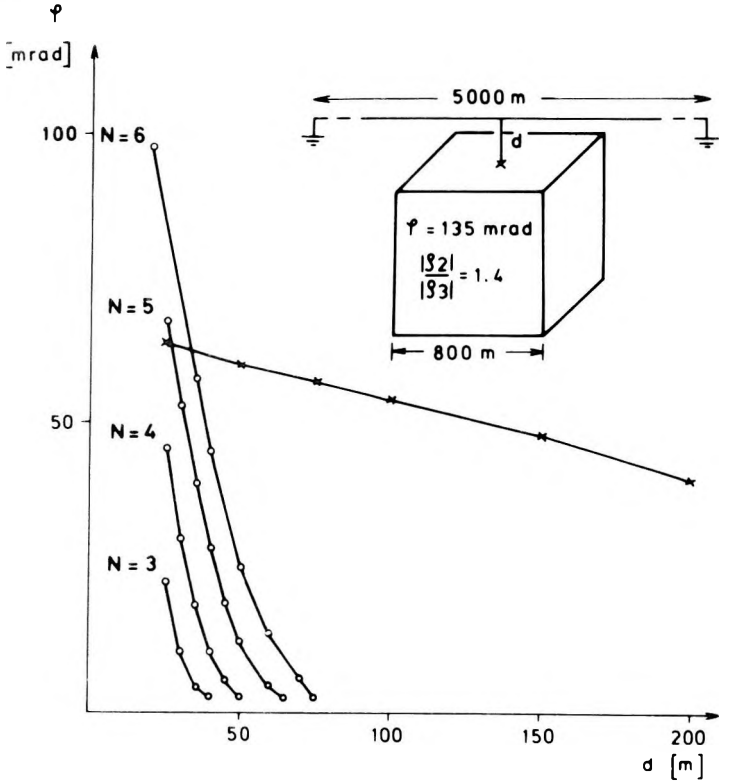

Fig. 8. Magnitude of phase anomaly as a function of depth to the upper surface for gradient array (x) and dipole–dipole array for different values of dipole separations *Na* (o)

8. ábra. A fázis-anomália nagysága a ható felső határfelülete mélységének függvényében, gradiens elrendezés (x) és különböző dipól távolságú *(Na)* dipól–dipól elrendezések (o) esetén

Рис. 8. Значения аномалий фазы в зависимости от глубины верхней кромки тела. Градиентная установка (x) и диполь–диполь установки с разными расстояниями *(Na)* между диполями (o)

The numerical calculations presented indicate that the properties of the electrode arrays used to study the geological structures in the field are very different from one another. It is important that the responses to different electrode arrays be computed for different models; only this ensures that the optimal configuration is used when prospecting for any expected ore type.

The gradient array is preferred when searching for a large body because of its good depth penetration in that case. Since, however, an anomaly is attenuated very gradually with increasing depth to the upper surface, it is difficult to interpret the depth to the upper surface from the measuring data.

The response of the dipole–dipole array on the other hand is attenuated rapidly with increasing depth to the upper surface, which makes it highly appropriate for establishing the depth to the upper surface as long as the dipoles can be sufficiently far apart. In practice, however, with large values of N the primary field of the dipole–dipole array is weak and so its use in surveying is hindered by the high transmitter output required.

In the case of a thin, vertical slab the IP anomaly is considerably smaller when measured with the gradient array than with the dipole–dipole array, especially at the high conductivity contrast values. On the other hand, the gradient array is very suitable for interpreting the dip whereas the dipole–dipole array is rather insensitive to the variation in dip.

Conductive overburden substantially attenuates the response of galvanic methods measured on the surface because a large part of the current passes through the overburden.

We can conclude that each particular geological problem can be solved best with one particular electrode system. Hence the program package described can be used not only in the interpretation of measuring data but also when planning the survey to find out the measuring system most appropriate for the problem.

REFERENCES

Eloranta E. 1984: A method for calculating mise-à-la-masse anomalies in the case of high conductivity contrast by the integral equation technique. Geoexploration, **22,** 2, pp. 77–88

Eskola L. 1979: Calculation of galvanic effects by means of the method of sub-areas. Geophysical Prospecting, **27,** 3, pp. 616–627

Eskola L., Hongisto H. 1981: The solution of the stationary electric field strength and potential of a point current source in a $2\frac{1}{2}$ dimensional environment. Geophysical Prospecting **29,** 2, pp. 260–273

Gradshteyn I. S., Ryzhik I. M. 1965: Table of integrals, series and products. Academic Press

Pelton W. H., Sill W. R., Smith B. D. 1983: Interpretation of complex resistivity and dielectric data part I. Geophysical Transactions, **29,** 4, pp. 297–330

Soininen H. 1984: The behavior of the apparent resistivity phase spectrum in the case of a polarizable prism in an unpolarizable half-space. Geophysics, **49,** 9, pp. 1534–1540

Soininen H. 1985: The behavior of the apparent resistivity phase spectrum in the case of two polarizable media. Geophysics, **50,** 5, pp. 810–819

Van Nostrand R. G., Cook K. L. 1966: Interpretation of resistivity data. U.S. Geol. Survey Professional Papers No. 499

KÉTRÉTEGES FÉLTÉRBEN LEVŐ DŐLT PRIZMA GALVANIKUS ANOMÁLIÁINAK SZÁMÍTÁSA

Heikki SOININEN

A cikk a látszólagos ellenállás- és gerjesztett polarizációs anomália numerikus modellezésére használható számítógépes programot ismertet. A tér számítását integrálegyenlet módszerrel oldja meg. Az alapvető modell a kétréteges féltérben lévő dőlt prizma. Valamennyi szereplő ellenállás lehet komplex és frekvenciafüggő, így lehetséges a szélessávú gerjesztett polarizációs módszer modellezése. Az ellenállás frekvenciafüggő értékeit vagy közvetlenül kőzetfizikai mérések alapján adhatjuk meg a programban, vagy egy matematikai diszperziós modellel adjuk meg a frekvenciafüggést.

A gradiens- és dipól–dipól elrendezéssel kapott anomáliákat hasonlítja össze különböző földtani szerkezetek esetén. A dipól–dipól elrendezéssel jobban ki lehet mutatni egy vékony, függőleges testet, mint a gradiens elrendezéssel, mert nagyobb az anomália, a dőlést viszont a gradiens elrendezéssel lehet jobban meghatározni.

Nagyméretű ható esetén a gradiens elrendezéssel kapott anomália csak lassan csökken a gerjeszthető test mélységének növekedésével. Ezért nagy testek kutatására sokkal alkalmasabb, mint a dipól–dipól elrendezés, ezen utóbbival viszont jobban meg lehet határozni a gerjeszthető test felső határfelületének mélységét.

A jól vezető fedő az áramkanalizáció révén jelentősen csökkenti a felszínen, galvanikus módszerekkel mérhető anomáliákat.

ВЫЧИСЛЕНИЕ АНОМАЛИЙ СОПРОТИВЛЕНИЯ И ВЫЗВАННОЙ ПОЛЯРИЗАЦИИ НАД НАКЛОННОЙ ПРИЗМОЙ, ВМЕЩАЮЩЕЙ В ДВУХСЛОЙНОЙ СРЕДЕ

Хэикки СОИНИНЕН

Представляется программа для вычисления цифровым моделированием аномалий кажущегося удельного сопротивления и вызванной поляризации. Поле вычисляется методом интегральных уравнений над наклонной призмой, вмещающей в двухслойной среде. Все сопротивления могут быть комплексными и зависящими от частоты, благодаря чего возможно моделирование метода вызванной поляризации в широком интервале частот. Значения сопротивлений, зависящие от частот могут быть даны в программе на основе измерений физических параметров пород, или их зависимость от частоты моделируется математическим способом.

Сопоставляются аномалии, полученные градиентной и диполь–диполь установками над разными геологическими структурами. Вертикальное тонкое тело по аномалиям диполь–диполь установки отражается более четко, чем по аномалиям градиентной установки, а падение тела лучше отражается аномалиями градиентной установки.

При объекте большого размера аномалия, измеренная градиентной установкой, с увеличением глубины объекта уменьшается только медленно. Поэтому градиентная установка более пригодна для исследования больших тел, чем диполь–диполь установка. Однако диполь–диполь установкой надежнее определяется глубина верхней кромки поляризующегося объекта.

Покрывающий слой с большой проводимостью существенно уменьшает аномалии, измеряемые на поверхности земли кондуктивным способом.

GEOPHYSICAL TRANSACTIONS 1985
Vol. 31. No. 4. pp. 373–389

A FEW UNSOLVED PROBLEMS OF APPLIED GEOPHYSICS

Gábor KORVIN*

The paper describes eight unsolved problems, stemming from statistical geophysics or rock physics: computation of effective physical properties in fluid-filled sedimentary rock (*Problems 1, 2*); dependence of the absorption coefficient of sound waves in heterogeneous rocks on the randomness of the rock (*Problems 3, 4*); fluctuation of the signal characteristics propagating through random media (*Problem 5*); computation of the reflected energy from an infinite, randomly dissipative half-space (*Problem 6*); and the statistical properties of the seismic signals, backscattered from randomly uneven boundaries (*Problems 7, 8*). In all cases basic references are provided and applications pointed out.

Keywords: rock physics, sedimentary rocks, wave propagation, seismic data processing

Introduction

I shall briefly describe – somewhat in the vein of RUELLE's "Five Turbulent Problems" [1983] – eight loosely connected puzzles, all stemming from statistical geophysics or rock physics. In all cases I provide the basic references for further work, including the history, motivation and possible applications of the problem. This paper is an outgrowth of a lecture held in 1982 at the Geology Department of the University of Houston; I dedicate it to the memory of Milton B. Dobrin, (1915–1980), late Professor of that Department, Man, Teacher, Geophysicist.

1. Hierarchy of velocity equations: generalized mixture rules

The first problem is frequently encountered in geophysics, rock physics and solid state physics.

Suppose we are given a composite material of volume V consisting of two phases of the respective volume fractions P, Q; $P+Q = V$, and suppose these constituents are uniformly distributed within the total volume. Suppose g is some physically measurable property that assumes the values g_1 and g_2, respectively, for the two constituents, and a value $\bar{g}$ for the composite. Suppose, further, that the value of $\bar{g}$ is unambiguously determined by the volume fractions P, Q and the specific properties g_1, g_2:

$$\bar{g} = M(g_1, g_2, P, Q) \tag{1}$$

* Eötvös Loránd Geophysical Institute of Hungary, POB 35, Budapest, H–1440
Manuscript received: 1 July, 1985

In KORVIN [1982a] it is shown that, if a set of physically plausible conditions is met, the only possible functional form of $M(g_1, g_2, P, Q)$ is the "general mixture rule"

$$M(g_1, g_2, P, Q) = \{\Phi g_1^t + (1-\Phi) g_2^t\}^{1/t} \tag{2}$$

for some real t, $t \neq 0$, or

$$M(g_1, g_2, P, Q) = g_1^{\Phi} g_2^{1-\Phi} \tag{3}$$

which follows from Eq. (2) by l'Hôspital's rule for $t=0$. In Eqs. (2), (3), Φ is porosity, defined as $\Phi = P/(P+Q)$. The general mean values have the very important property [cf. BECKENBACH and BELLMAN 1961 § I.16] that for $g_1, g_2 > 0$, $\Phi \neq 0$, $\Phi \neq 1$ and $g_1 \neq g_2$ the expression $\{\Phi g_1^t + (1-\Phi) g_2^t\}^{1/t}$ is a strictly monotonously increasing function of t in $(-\infty, \infty)$.

In case of sound speeds, e.g., in fluid-filled sedimentary rocks the general rules (2), (3), contain, in particular, the following widely used "velocity formulae":

- for $t=-2$ the "approximate Wood equation" [WATERMAN and TRUELL 1961, KORVIN 1977a, 1978 b];
- for $t=-1$ the "time-average" equation [WYLLIE et al. 1956];
- for $t=0$ the "vugular carbonate" formula [of MEESE and WALTHER 1967];
- for $t=1$ the average velocity formula [BERRY 1959].

TEGLAND's [1970] method of sand–shale ratio determination also assumes a $t=-1$ time average equation; MATEKER's [1971] effective attenuation factor in an alternating sequence of thick sand–shale layers is a linear weighted (i.e. $t=1$) combination of the specific attenuations, further examples from different fields of geophysics are to be found in KORVIN [1978b, 1982 a].

The functional forms (2), (3) are derived in KORVIN [1982a] from the following set of physically plausible conditions. (The derivation is based on the theory of functional equations, particularly on the results of ACZÉL [1961].)

Condition 1. reflexivity

$$M(g_1, g_1, P, Q) = g_1 \quad \text{for all } P, Q \ (P+Q > 0) \tag{4}$$

Condition 2. idempotency

$$M(g_1, g_2, P, 0) = g_1 \quad \text{for all} \quad P > 0 \tag{5}$$

$$M(g_1, g_2, 0, Q) = g_2 \quad \text{for all} \quad Q > 0 \tag{6}$$

Condition 3. homogeneity (of 0-th order) with respect to the volume fractions

$$M(g_1, g_2, P, Q) = M(g_1, g_2, \lambda P, \lambda Q) \tag{7}$$

$$\text{for all } P, Q, \lambda \quad \text{such that} \quad P+Q > 0, \quad \lambda > 0$$

Condition 4. internity. The property $\bar{g}$ measured on the composite lies between the specific values g_1, g_2 of the constituents; if $g_1 < g_2$, say, then for $P+Q > 0$:

$$M(g_1, g_2, 1,0) \leq (g_1, g_2, P, Q) \leq M(g_1, g_2, 0,1) \tag{8}$$

Condition 5. bi-symmetry (this concept is due to ACZÉL [1946]). Given two composites, the first consisting of P_1 and Q_1 parts of materials of g_1 and g_2 properties; the second of P_2 and Q_2 parts of materials of G_1 and G_2 properties, the following two expressions for the measured property $\bar{g}$ of the four-component aggregate must be equal:

$$\begin{aligned} &M[M(g_1, g_2, P_1, Q_1); M(G_1, G_2, P_2, Q_2); P_1+Q_1; P_2+Q_2] = \\ &= M[M(g_1, G_1, P_1, P_2); M(g_2, G_2, Q_1, Q_2); P_1+P_2; Q_1+Q_2) \end{aligned} \tag{9}$$

Condition 6. monotonicity with respect to the volume fractions.

$$\text{If } g_1 < g_2, \quad \text{say,} \quad P+Q_1 > 0, \quad Q_2 > Q_1$$

$$\text{then} \quad M(g_1, g_2, P, Q_1) < M(g_1, g_2, P, Q_2) \tag{10}$$

Condition 7. monotonicity with respect to the physical properties.

$$\text{If } P+Q > 0, \quad g_2 < g_3 \quad \text{then} \quad M(g_1, g_2, P, Q) < M(g_1, g_3, P, Q) \tag{11}$$

Condition 8. homogeneity (of first order) with respect to the physical properties

$$\begin{aligned} &M(\lambda g_1, \lambda g_2, P, Q) = \lambda M(g_1, g_2, P, Q) \\ &\text{for all} \quad P, Q, \lambda \quad \text{such that} \quad P+Q > 0, \quad \lambda > 0 \end{aligned} \tag{12}$$

In KORVIN [1982a] it is proved that if the function $M(g_1, g_2, P, Q)$ defining the effective physical property $\bar{g}$ of a two-component material satisfies Conditions 1–8 (Eqs. 4–12) then

$$\bar{g} = M(g_1, g_2, P, Q) = \{\Phi g_1^t + (1-\Phi) g_2^t\}^{1/t}$$

$$\text{for some real} \quad t, t \neq 0, \quad \Phi = \frac{P}{P+Q} \quad \text{or} \quad g = g_1^{\Phi} g_2^{1-\Phi}.$$

In case of sound speeds, e.g. in sandstone, *Fig. 1* shows porosity–velocity curves for different values of the parameter t ($g_1 = v_{fluid} = 1545$ m/s; $g_2 = v_{matrix} = 5542$ m/s, after MEESE and WALTHER 1967; the Berea, Boise, Miocene, Page sandstone data are taken from MEESE and WALTHER [1967], the Texas data from HICKS and BERRY [1956]). It is seen from Fig. 1 that the sandstone data are best fitted by a $t = -0.6$ curve, i.e. by the formula

$$\bar{v} = \{\Phi \cdot v_{fluid}^{-06} + (1-\Phi) v_{matrix}^{-06}\}^{-1/0.6}$$

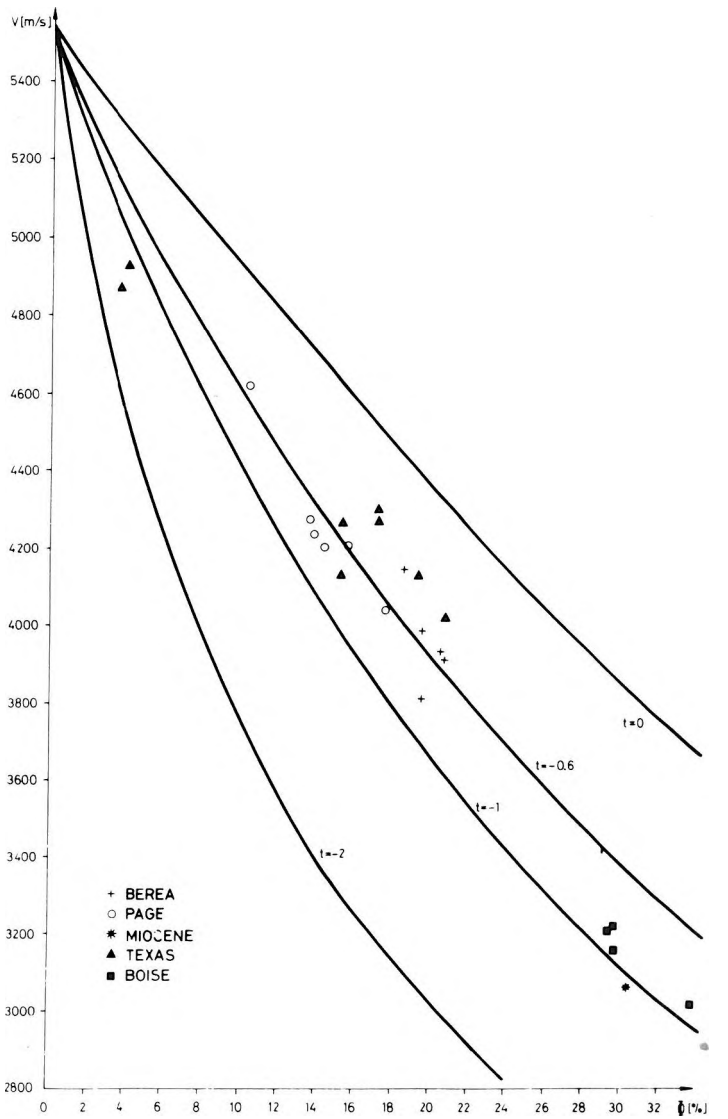

Fig. 1. Porosity–velocity master curves for sandstone [From KORVIN 1978b]

1. ábra. Porozitás–sebesség görbesereg homokkövekre [KORVIN 1978b-ből]

Рис. 1. Кривые зависимости скорости от пористости для песчаниках [По KORVIN 1978b]

Thus, we are led to *Problem 1*: What is the physical meaning (if any) of the parameter t in Eq. 2? Does $t = -0.6$ have any particular meaning for sandstone?

There is also another, variational approach, for the determination of the effective properties of composite materials, culminating in the celebrated HS [HASHIN-SHTRIKMAN, 1963] bounds on the effective properties in terms of the specific ones. A very recent summary of the topic, with many references, is HUGHES and PRAGER [1983], see also STELL [1983]; the standard reference for earlier work is HASHIN [1964].

It would be nice to see somebody solve *Problem 2*, that is, to reconcile the functional equation approach [of KORVIN 1978b, 1982a] with the HS variational approach, or at least to use HS bounds to derive non-trivial bounds for t.

2. Sound absorption and rock entropy

In 1978 BELTZER studied elastic wave propagation in randomly porous materials. He concluded that "for low frequency regimes the randomness of porosity leads to an increase in the attenuation and dispersion of the elastic wave".

BELTZER's result is highly plausible and in agreement with the general understanding that the heterogeneity of a medium causes additional dissipation of the propagating elastic wave. (It is well known, for example, that the sound attenuation in crystalline materials is less for a single crystal than for an aggregate; [BRADLEY and FORT 1966].) Prior to BELTZER's work similar conclusions had already been reported by the present author, in connection with elastic waves propagating in a random stack of layers (the hypothesis was published in 1976, its heuristic proof in 1978c). KORVIN [1980] applies stochastic perturbation methods of random wave propagation theory [KELLER 1964, KARAL and KELLER 1964] in order to generalize BELTZER's results for rocks of random structure. In KORVIN [1980] it is shown that in multicomponent rocks the low-frequency attenuation coefficient is proportional to (more exactly, positively correlated with) the quantity

$$E = -\sum_{i=1}^{n} p_i \log p_i \tag{13}$$

where p_i ($i = 1, \ldots, n$) is the relative volume ratio of the i-th phase, $\Sigma\, p_i = 1$. The quantity E, however, measures the randomness of the constitution of the rock and, in Russian literature, is termed "rock entropy" [cf. BYRYAKOVSKIY 1968]. Recalling that in the statistical theory of phase transitions of disordered systems the entropy of a random aggregate of several components always consists of two parts

$$S = S_{configurational} + S_{mixture} \tag{14}$$

where $S_{mixture}$ has the same form as the entropy E in Eq. (13). Eq. 14 is the so-called Flory–Huggins formula, [see ZIMAN 1979, §. 7.2.], we immediately see *(Problem 3)* that either the concept of rock entropy should carefully be redefined, or the random wave equation solved more precisely in order to decide whether or not the attenuation depends on the configurational part of rock entropy.

The hypothetical connection between attenuation and randomness (entropy) of the rock presents us with a further, much more delicate problem.

It is well known that frequency-dependent attenuation and velocity dispersion lead to a distortion of propagating acoustic pulses; BARKHATOV [1982, §. 3.6.4.] and BARKHATOV and SHMELEV [1969] even speak about the changes of signal entropy during hydroacoustic propagation. KUZNETSOV et al. [1973] and HOLLIN and JONES [1977] propose that the correlation between the propagating pulses for the determination of the attenuation characteristics be measured. Theoretically, the propagation of the two-point correlation function (as of any other quadratic quantities) can be described by the Bethe–Salpeter equation [BOURRET 1962] or by appropriate transport equations [see e.g. BUGNOLO 1960]. In connection with the latter approach FRISCH [1968 p. 145] comments: "...there are some physical difficulties in the interpretation of the solution, which have not been settled yet. It appears, for example, that in contradistinction to the homogeneous nonrandom case, there is an energy loss, even when the medium is not dissipative."

It seems to us that this problem, together with that concerning the interconnection of attenuation and randomness, can be solved by following up the pioneering ideas of CASTI and TSE; these authors showed in 1972 that the Kalman–Bucy optimal filtering theory and radiative transfer theory "which from a physical point of view seem to have very little in common, may be brought together by careful examination of their respective initial value formulations" [*op. cit.* p. 42].

In their concluding remarks CASTI and TSE [1972 p. 53] state: "In conjunction with the active filtering problem, let us mention a radiative transfer function ...this is the absorption function which is defined by means of conservation law, i.e. it corresponds to the radiative energy which is input to the atmosphere, but which is neither transmitted through nor reflected back out... In the active filtering case there is reason to suspect that this function may correspond to a loss of inherent information in the known control input due to interaction with the noisy system. If this correspondence can be made precise, it would seem to be possible to establish a conservation of information law for stochastic systems".

That is, we can state our *Problem 4* as: Derive attenuation in random media from "conservation of information" principles!

3. Ignorance versus depth: the turbidity factor paradox

One of the basic results of seismic wave propagation in randomly inhomogeneous media is that velocity- and density inhomogeneities cause scattering of waves, the scattered waves are superimposed on the primaries and lead to amplitude and phase fluctuations in the observed wave pattern. We shall neglect density fluctuations and assume that an acoustic wave of frequency f propagates along a distance $AB = L$ in a random medium where sound-speed randomly fluctuates around some constant C_0 as

$$C = \frac{C_0}{1+\varepsilon} \tag{14}$$

where

$$\langle\varepsilon\rangle = 0, \langle\varepsilon^2\rangle \ll 1, R_{\varepsilon\varepsilon}(r) = \langle\varepsilon(\mathbf{x})\varepsilon(\mathbf{x}+\mathbf{r})\rangle = \\ = \langle\varepsilon^2\rangle \exp[-|r/r_0|] \quad (r = |\mathbf{r}|),$$

r_0 is the correlation distance of the inhomogeneities. Denoting mean transit time L/C_0 by T, its fluctuation by ΔT and mean wavelength by λ, it can be shown that, if $r_0 \gg \lambda$:

$$\langle(\Delta T)^2\rangle = \frac{L}{C_0^2}\langle\varepsilon^2\rangle r_0\sqrt{\pi} \tag{15}$$

(see CHERNOV [1960], or KORVIN [1973] for a more general case). The gist of Eq. (15) is that the square of the fluctuation of transit times linearly increases with the distance travelled. To show a practical example of Eq. (15), let us recall the classical paper of GRETENER [1961] who analysed the deviations between the integrated travel times computed from conventional and continuous velocity loggings in wells. The deviations found by him consisted of a systematic and a random part. The systematic deviations were ascribed, in a much-discussed paper of STRICK 1971, to velocity dispersion while the random scattering was found to increase with the square root of the distance travelled by the seismic wave (in accordance with Eq. (15), see *Fig. 2*).

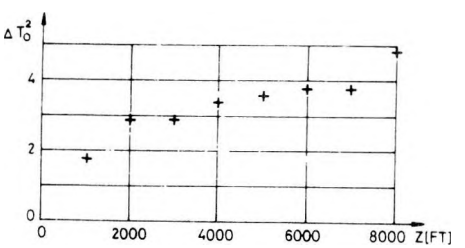

Fig. 2. Scattering of arrival times. [After GRETENER 1961]

2. ábra. A beérkezési idők szórása [GRETENER 1961 után]

Рис. 2. Отклонения времен вступления [По GRETENER 1961]

The companion formula to Eq. (15) refers to the logarithmic amplitude fluctuation of the propagating waves and states that

$$\left\langle \left(\Delta \log \frac{A}{A_0} \right)^2 \right\rangle = g \cdot L \tag{16}$$

where A_0 is wave-amplitude in the homogeneous medium and g is a function, which possibly also depends on frequency, correlation distance, etc.

The factor g is termed "inhomogeneity factor", or "turbidity factor" ([GALKIN and NIKOLAEV 1968, NIKOLAEV and TREGUB 1970]; the definitive monograph on the subject is [NIKOLAEV 1973]).

A great number of studies have been carried out in seismology to determine the inhomogeneity of the crust and upper mantle using time- or logarithmic amplitude fluctuation, or both [AKI 1973, CAPON 1974, BERTEUSSEN et al. 1975, etc]; most recently by POWELL and MELTZER [1984]; a similar study in reflection seismics was carried out by KORVIN [1977b]. For exploration geophysicists, the message of Eqs. (15), (16) is that the error of the seismic measurements linearly increases with the depth studied (as was observed by POSGAY as early as 1954) i.e. our ignorance about the Earth linearly increases with depth! This triumphant feeling of ignorabimus has recently been shattered by the fascinating model experiments reported by Gertrude NEUMANN and K. SCHIEL in 1977. NEUMANN and SCHIEL prepared more than 20 two-dimensional models (somewhat in the vein of LEVIN and ROBINSON [1969]) consisting of 2000 × 800 mm macrolon and 2000 × 1200 mm perspex plates with inhomogeneities quasi-randomly arranged in rows *(Fig. 3)*. They estimated the logarithmic amplitude fluctuation and computed the turbidity factor assuming the validity of Eq. (16) (where L should be substituted by the number of "rows" of inhomogeneities in the model). Their results are reproduced in *Fig. 4*, for one family of the macrolon models. The estimated g factor first increases with the number of rows N, then begins to decrease, i.e. instead of (16), they found a

$$\left\langle \left(\Delta \log \frac{A}{A_0} \right)^2 \right\rangle = g \cdot L^{\alpha} \tag{17}$$

law, for greater distances with an exponent α less than 1. This, of course, reminded NEUMANN and SCHIEL of Brownian motion or diffuse multiscattering (*op. cit.* p. 225).

Since these model experiments are extremely well-documented, it is worth while to call the reader's attention to this paper and to pose *Problem 5* as: Explain quantitatively the findings of NEUMANN and SCHIEL [1977] in terms of diffuse multiscattering! The problem becomes even more important since a very recent paper of POWELL and MELTZER [1984] has cast renewed doubts on the overall applicability of the CHERNOV- (i.e. NIKOLAEV-, i.e. RYTOV-) method.

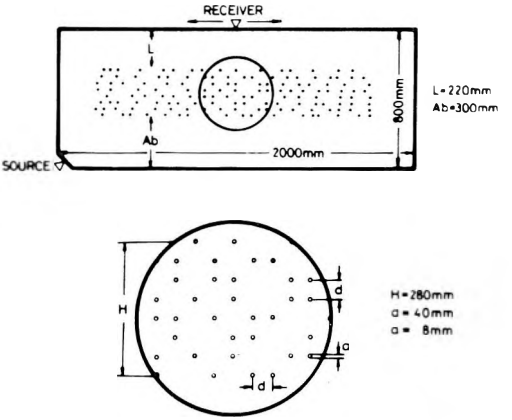

Fig. 3. Structure and model parameters used in the experiments of NEUMANN and SCHIEL [1977]

3. ábra. Felépítési- és modell-paraméterek NEUMANN és SCHIEL [1977] kísérleteiben

Рис. 3. Параметры строения и модели в экспериментах NEUMANN-a и SCHIEL-a [1977]

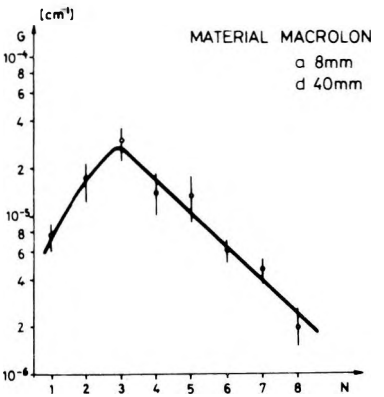

Fig. 4. Dependence of the turbidity factor G on the number of rows N in one of the NEUMANN–SCHIEL macrolon models. [After NEUMANN and SCHIEL 1977]

4. ábra. G turbiditás-faktor függése N sorszámtól, NEUMANN és SCHIEL egyik makrolon modelljében. [NEUMANN és SCHIEL 1977 után]

Рис. 4. Зависимость фактора мутности G от номера N, на макролонной модели NEUMANN-a и SCHIEL-a. (По NEUMANN и SCHIEL 1977)

4. Energy return from a dissipative half-space

There is an interesting theorem of ROBINSON and TREITEL [1965, 1966] which states that any series of parallel layers, characterized by an arbitrary sequence of reflection coefficients, which is bounded by a totally reflecting "wall" ($r = \pm 1$), completely reflects the incident energy in an infinite observation time. In [1977 a] KORVIN, in an attempt to generalize the Robinson–Treitel theorem, restated the problem in terms of a one-dimensional random walk of acoustic energy quanta, applied the invariant embedding technique of BELLMAN et al. [1958], and derived a partial integro-differential equation for the description of the total energy $U(t)$ reflected from a random infinite half-space in the time interval $(0, t)$. It was proved that for one-dimensional inhomogeneities, assuming a stationary sequence of random reflection coefficients and that the reflecting interfaces obey a Poisson distribution, the total incident energy is reflected from the inhomogeneous half-space during an infinitely long observation time. The asymptotic form of $U(t)$ is also given, in Eq. (79) of KORVIN [1977 a].

It turned out later that various formulations of this problem can be encountered in the most different branches of physics (in solid state physics, for example, the phenomenon is closely connected to the "localization theorems", see ZIMAN [1979, Chapter 8], or the recent summary of STEPHEN [1983].

The most ingenious proof of the total reflection by a semi-infinite random medium was given by SULEM and FRISCH [1972] [see also SULEM 1973] who used the Ricatti transformation to reduce the Helmholtz equation to a single-point boundary problem, observed that the complex impedance Z_N of a random stack of N layers constitutes a kind of "random walk" on the half-plane C^+ ($Im\, z > 0$) as the number N of layers is gradually increased, and used the ergodic theory of dynamic systems [ARNOLD and AVEZ 1967, HALMOS 1956] to prove total reflection.

Of course, ergodic theory gives no indication as to the rate of development of a system towards its equilibrium. The Monte Carlo computer simulations in SULEM and FRISCH [1972], however, suggest that the mean reflection coefficient exponentially converges to one, rather similarly to the asymptotic Eq. (79) in KORVIN 1977a.

In SULEM and FRISCH [*op. cit.*, p. 225] there is posed the important problem connected with the more realistic case of a slightly dissipative medium which, obviously, cannot be totally reflecting. Computer simulations *(Fig. 5)* indicate that the Césaro means of the reflection coefficients

$$\frac{1}{N} \sum_{n=0}^{N-1} |r_N|$$

still converge, but more slowly than for a non-dissipative half-space, and to a finite limit less than one. Unfortunately, the ergodic theory, used by SULEM and FRISCH for the nondissipative case, does not apply if we assign complex values

to the refractive index since the measure corresponding to the random walk of the complex impedance Z_N will not be invariant any more.

At the same time, in the dissipative case, the integro-differential equation in KORVIN [1977] will also yield divergent solutions. Thus, it seems justifiable to invite the reader to solve *Problem 6*, i.e. to generalize the theorem of ROBINSON and TREITEL and compute the energy returned from a, finite or infinite, stack of random dissipative layers!

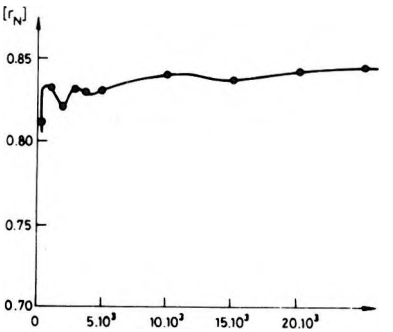

Fig. 5. Césaro mean of the reflection coefficient in a randomly alternating stack of two slightly dissipative layers with the refractive indices $n_1 = 2 + 5i \cdot 10^{-3}$ and $n_2 = 5 + 5i \cdot 10^{-3}$, respectively, and with a mean layer thickness of unity. [After SULEM and FRISCH 1972]

5. ábra. Két, enyhén disszipatív réteg véletlenszerűen váltakozó sorának reflexiós koefficienseiből képezett Césaro átlag. A törésmutatók: $n_1 = 2 + 5i \cdot 10^{-3}$, ill. $n_2 = 5 + 5i \cdot 10^{-3}$, az átlagos rétegvastagságok egységnyiek. [SULEM és FRISCH 1972 után]

Рис. 5. Среднее Césaro полученное из коэффициентов отражений случайно изменяющегося множества двух слабодиссипативных слоев. Коэффициенты преломления: $n_1 = 2 + 5i \cdot 10^{-3}$; $n_2 = 5 + 5i \cdot 10^{-3}$, средняя мощность слоев составляет единицу. [По SULEM и FRISCH 1972]

5. Langleben's phenomenon and the diffuse reflection shadow

It has long been a basic problem of Hungarian reflection seismics that in many cases we can get only intricate diffuse reflections from the uneven surface of the basement [SZÉNÁS and ÁDÁM 1953]. Due to these diffuse reflections it is rather difficult at some places to map the basin floor accurately: diffraction arrivals coming from the surface unevennesses follow the basement reflection as a "diffuse shadow" of a few hundred ms length so that it tends to be very difficult to detect eventual deeper reflections. In marine seismic profiling, similar difficulties were reported by CLAY and RONA [1964]. The existence of the diffuse reflection shadow following rough boundaries has also been demonstrated by model experiments [VOSKRESENSKY 1962, LEONG et al. 1971]. For a special

non-differentiable random surface model the time-behaviour of the diffuse reflection shadow was theoretically investigated in the low-frequency limit by BIOT [1957]; for Gaussian differentiable random surfaces, and in the high-frequency limit, by KORVIN [1982b]. Recent interest in the topic is indicated by TSAI [1984] who proposes special CDP stack and velocity filtering techniques to reduce coherent scattered noise.

In 1970 LANGLEBEN reported a very strange series of experiments, carried out under the ice cover in Tanquary Fiord, Ellesmere Island, NW Territories, Canada. He measured the specular reflection of water-borne sound at the water–sea-ice interface as a function of the angle of incidence and of frequency. The geometrical configuration of his measurement is reproduced in *Fig. 6* (the frequency varied from 20 kHz to 450 kHz). His results *(Table I)* do not show any systematic change of the specular reflection coefficient with frequency. The "striking insensitivity of back-scattering to frequency", in cases when the scales of irregularities range from many times smaller to many times greater than the radiation wavelength, had also been observed by MARSH [1961, p. 332]. Note that the dendritic growth of ice very likely also results in such an ill-defined phase-boundary of fractal geometry [cf. BRADY and BALL 1984], containing irregularities at all scales. (The possible fractal nature of the underside of sea ice was first observed by ROTHROCK and THORNDIKE [1980]; see also their more recent paper [1984].)

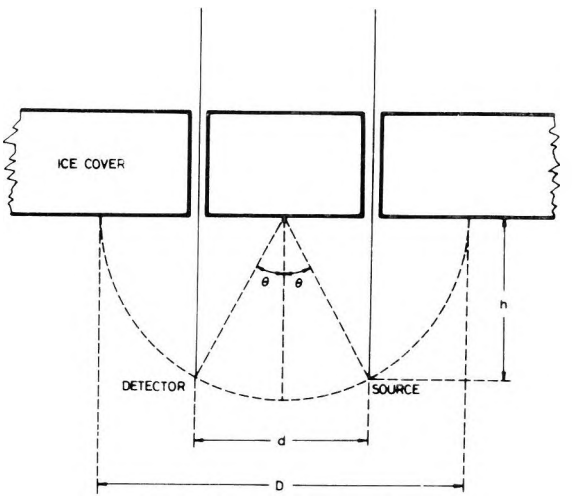

Fig. 6. Geometrical configuration of Langleben's experiment. Source and detector move along the semicircle indicated. [After LANGLEBEN 1970].

6. ábra. Langleben kísérletének geometriai elrendezése. Adó és vevő egy félkörön mozog. [LANGLEBEN 1970 után]

Рис. 6. Геометрия эксперимента LANGLEBEN-а. Датчик и приемник движутся на одном полукруге. [По LANGLEBEN 1970]

Table I. Amplitude of reflection coefficients at the water–sea-ice interface [after LANGLEBEN 1970]

Frequency	Angle of incidence [degree]				
kHz	15	30	45	60	75
17.9	0.24	0.20	0.48	0.36	0.88
23.1	0.091	0.034	0.18	0.41	0.51
24.8	0.13	0.070	0.29	0.63	0.38
47.0	0.056	0.17	0.89	0.89	1.22
56.5	0.083	0.25	0.42	0.75	0.75
89.9	0.039	0.053	0.41	0.63	0.96
118	0.13	0.16	0.72	0.88	1.06
126	0.055	0.036	0.32	0.69	0.81
184	0.056	0.11	0.56	0.75	0.97
227	0.021	0.005	0.43	0.44	0.91
332	0.17	0.22	0.019	0.50	0.45
387	0.083	0.091	0.36	0.16	1.00
435	0.066	0.088	0.016	0.11	0.94

The surprising feature of LANGLEBEN's data is that, when averaged over frequency, the mean reflection coefficients become a reasonably smooth function of the angle of incidence *(Fig. 7)*. Since, using the jargon of data processing, averaging over frequencies is equivalent to a deconvolution operation in the time domain, LANGLEBEN's results suggest the hypothesis *(Problem 7)*, that a suitable generalization of the single- or multichannel deconvolution procedure could be profitable in the elimination of the diffuse reflection shadow.

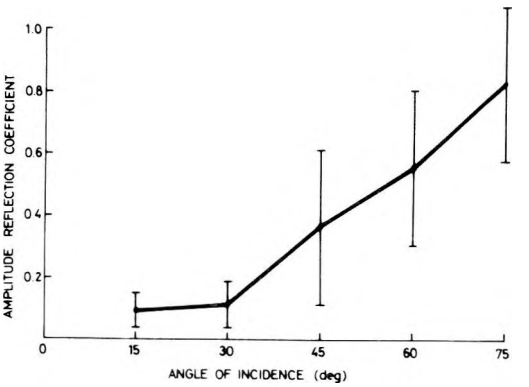

Fig. 7. Amplitude reflection coefficient of water-borne sound waves reflected at the underside of the sea ice cover, as a function of angle of incidence. [After LANGLEBEN 1970]

7. ábra. A tengert borító jég alsó határfelületéről visszavert hanghullámok reflexiós koefficiense a beesési szög függvényében. [LANGLEBEN 1970 után]

Рис. 7. Коэффициент отражения звуковых волн, отражающихся от нижней поверхности границы льда, покрывающего море, в зависимости от угла падения. [По LANGLEBEN 1970]

In the single-channel solution it should be recalled that the diffuse "reverberated" signal is very likely not minimum-phase [see KORVIN 1982b], i.e. the deconvolution filter must be specially designed (as, for example, in RISTOW and JURCZYK [1975]). The design of the multi-channel filter for the removal of the diffuse reflection shadow could very likely be made along the general lines described in BACKUS et al. [1964]. For the estimation of the horizontal and temporal correlations of the diffuse noise, that is necessary for the design of the optimum multichannel filter, use should be made of the results in LEVIN and ROBINSON [1969], DUNKIN [1969], KORVIN [1978a]. It goes without saying that a physical explanation of LANGLEBEN's phenomenon (i.e. why is the frequency-averaged backscattering coefficient equal to the backscattering coefficient of an effective smooth surface, at least for a certain kind of random surfaces?) is still badly needed and it is posed here as *Problem 8*.

* * *

The main ordering principle behind this set of problems has been my continuous interest in the last 15 years in applying random wave propagation concepts and statistical ideas to the physics of sedimentary rocks. I do hope my readers will find some of these problems sufficiently interesting so as to solve them – as I called for in the original title of this lecture: *"A few problems I'd like to see solved"*.

REFERENCES

ACZÉL J. 1946: The notion of mean values. Nor. Vidensk. Selsk. Forh., **19**, 83–86

ACZÉL J. 1961: Vorlesungen über Funktionalgleichungen und ihre Anwendungen. VEB Deutscher Verlag der Wissenschaften, Berlin

AKI K. 1973: Scattering of P-waves under the Montana LASA. J. Geoph. Res. **78**, No 8, pp. 1334–1346

ARNOLD V. I., AVEZ A. 1967: Problems ergodiques de la mécanique classique. Gauthier–Villars, Paris.

BACKUS M., BURG J., BALDWIN D., BRYAN E. 1964: Wideband extraction of mantle P-waves from ambient noise. Geophysics, **29**, 5, pp. 672–692

BARKHATOV A. N. 1982: Modelling of the propagation of sound waves in the oceans (In Russian). Hydrometeoizdat, Leningrad

BARKHATOV A. N., SHMELEV I. I. 1969: A study of the under-surface sound channel as communication channel, under model conditions (In Russian). Akust. Zhurnal **15**, 2

BECKENBACH E. F., BELLMAN R. 1961: Inequalities. Springer Verlag, Berlin–Göttingen–Heidelberg.

BELLMAN R., KALABA R., WING G. M. 1958: On the principle of invariant imbedding and neutron transport theory, I. – One-dimensional case. J. Math. Mech. **7**, No 2, pp. 149–162; II – Functional equations: *ibid* 7, No 5, pp. 741–756

BELTZER A. 1978: The influence of random porosity on elastic wave propagation. J. Sound Vibr. **58**, No. 2, pp. 251–256

BERRY J. E. 1959: Acoustic velocity in porous media. J. Pet. Technol., **11**, 10, pp. 262–270

BERTEUSSEN K. A., CHRISTOFFERSSON A., HUSEBYE E. S., DAHLE A. 1975: Wave scattering theory in analysis of P-wave anomalies at NORSAR and LASA. Geoph. J. R. Astr. Soc. **42**, No 2, pp. 403–417

BIOT M. A. 1957: Reflection on a rough surface from an acoustic point source. Journal Acoust. Soc. Am. **29,** No 11, pp. 1193–1200

BOURRET R. C. 1962: Stochastically perturbed fields, with applications to wave propagation in random media. Nuovo Cimento, **26,** No. 1, pp. 1–31

BRADLEY J. J., FORT A. N. JR. 1966: Internal friction in rocks. In: Handbook of physical constants (Ed. CLARK, S. P. Jr.) Geol. Soc. Am. Memoir, No. 97, pp. 175–193

BRADY R. M., BALL R. C. 1984: Fractal growth of copper electrodeposits. Nature, **309,** 17, pp. 225–229

BUGNOLO D. S. 1960: Transport equation for the spectral density of a multiple scattered electromagnetic field. J. Appl. Phys. **31,** 7, pp. 1176–1182

BYRYAKOVSKY L. A. 1968: Entropy as criterion of heterogeneity of rocks. (In Russian). Soviet Geol. **3,** pp. 135–138

CAPON J. 1974: Characterization of crust and Upper Mantle structure under LASA as a random medium. Bull. Seism. Soc. Am. **64,** No 1, pp. 235–266

CASTI J., TSE E. 1972: Optimal linear filtering theory and radiative transfer: comparisons and interconnections. J. Math. Anal. Appl. **40,** pp. 45–54

CHERNOV L. A. 1960: Wave propagation in a random medium. Mc Graw–Hill, New York

CLAY C. S., RONA P. A. 1964: On the existence of bottom corrugations in the Blake-Bahama basin. J. Geoph. Res. **69,** 2, pp. 231–234

DUNKIN J. W. 1969: Scattering of a transient, spherical P-wave by a randomly inhomogeneous, elastic halfspace. Geophysics, **34,** 3, pp. 357–382

FRISCH U. 1968: Wave propagation in random media. In: Probabilistic methods in applied mathematics. I. (Ed. BHARUCHA-REID, A. T.) Academic Press, New York–London, pp. 75–198

GALKIN I. E., NIKOLAEV A. V. 1968: An attempt to study the turbidity of the Earth's crust and upper mantle according to the amplitudes of refracted waves (In Russian). Izv. AN SSSR, Ser. Fiz. Zemli, 8, pp. 36-47

GRETENER P. E. F. 1961: An analysis of the observed time discrepancies between continuous and conventional well velocity surveys. Geophysics, **26,** No 1, pp. 1–11

HALMOS P. R. 1956: Lectures on ergodic theory. Chelsea, New York

HASHIN Z. 1964: Theory of mechanical behaviour of heterogeneous media. Appl. Mech. Rev. **17,** No. 1, pp. 1–9

HASHIN Z., SHTRIKMAN S. 1963: A variational approach to the theory of the elastic behaviour of multiphase materials. J. Mech. Phys. Solids. **11,** pp. 127–140

HICKS W. G., BERRY J. E. 1956: Application of continuous velocity logs to determination of fluid saturation of reservoir rocks. Geophysics, **21,** 3, pp. 739–754

HOLLIN K. A., JONES M. H. 1977: The measurement of sound absorption coefficient in situ by a correlation technique. Acustica, **27,** No. 2, pp. 103–110

HUGHES B. D., PRAGER S. 1983: Random processes and random systems: an introduction. In: The mathematics and physics of disordered media. (Eds. B. D. HUGHES and B. W. NINHAM) Springer, Berlin–Heidelberg–New York–Tokyo, pp. 1–108

KARAL F. C. JR., KELLER J. B. 1964: Elastic, electromagnetic and other waves in a random medium. J. Math. Phys. **5,** No. 4, pp. 537–549

KELLER J. B. 1964: Stochastic equations and wave propagation in random media. Proc. Symp. Appl. Math. **16,** pp. 145–170

KORVIN G. 1973: Certain problems of seismic and ultrasonic wave propagation in a medium with inhomogeneities of random distribution. Geoph. Trans. **21,** Nos 1–4, pp. 5–34

KORVIN G. 1976: Seismic wave propagation in media of randomly inhomogeneous velocity distribution. 21. Geoph. Symp., Leipzig

KORVIN G. 1977a: Certain problems of seismic and ultrasonic wave propagation in a medium with inhomogeneities of random distribution, II. Wave attenuation and scattering on random inhomogeneities. Geophys. Trans., **24,** Suppl. 2, pp. 3–38

KORVIN G. 1977b: Estimation of the inhomogeneity of the earth from the fluctuation of the seismic signals. (A case history) (In Hungarian). Magyar Geofizika **18,** No. 4, pp. 134–149

KORVIN G. 1978a: Correlation properties of source generated seismic noise, scattered on velocity inhomogeneities. Acta Geod. Geoph. Mont. Acad. Sci. Hung. **13,** Nos 1–2, pp. 201–210

KORVIN G. 1978b: The hierarchy of velocity formulae: generalized mean value theorems. Acta Geodaet. Geophys. Mont. Acad. Sci. Hung. **13,** Nos 1–2, pp. 211–222

KORVIN G. 1978c: Wave attenuation in multicimponent rocks, a relation between the attenuation coefficient and the heterogeneity (entropy) of the rocks (In Hungarian). Magyar Geofizika, **18,** No. 3, pp. 106–116

KORVIN G. 1980: The effect of random porosity on elastic wave attenuation. Geophys. Trans. **26,** pp. 43–56

KORVIN G. 1982a: Axiomatic characterization of the general mixture rule. Geoexploration. **19,** pp. 267–276

KORVIN G. 1982b: Certain problems of seismic and ultrasonic wave propagation in a medium with inhomogeneities of random distribution. III. Statistics of the diffuse reflection shadow following a rough reflecting boundary. Geophys. Trans. **28,** 1, pp. 5–19

KUZNETSOV O. L., KAYDANOV E. P., RUKAVITSYN V. N. 1973: Some possibilities of the application of correlation analysis in sonic logging (In Russian). Trudy VNIYAG, **15,** pp. 56–59

LANGLEBEN M. P. 1970: Reflection of sound at the water – sea ice interface. Journal Geoph. Res., **75,** 27, pp. 5243–5246

LEONG W. K., KAN T. K., CLAY C. S. 1971: Use of acoustic scattering theory to interpret marine geophysical data. Univ. Wisconsin Geoph. and Polar Research Center, Research Rept. 71–7

LEVIN F. K., ROBINSON D. J. 1969: Scattering by a random field of surface scatterers. Geophysics, 34, No 2, pp. 170–179

MARSH H. W. 1961: Exact solution of wave scattering by irregular surfaces. Journal Acoust. Soc. Am., **33,** 3, pp. 330–333

MATEKER E. J. JR. 1971: Lithologic predictions from seismic reflections. Oil and Gas J. (Nov. 8. 1971) pp. 96–100

MEESE A. D., WALTHER H. C. 1967: An investigation of sonic velocities in vugular carbonates. 8th SPWLA Symp., Denver

NEUMANN G., SCHIEL K. 1977: Model investigations on inhomogeneous media. Publ. Inst. Geophys. Pol. Acad. Sci., A-4 (115), pp. 215–226

NIKOLAYEV A. V. 1973: Seismics of heterogeneous and turbid media. (in Russian). Nauka, Moscow

NIKOLAYEV A. V., TREGUB F. S. 1970: A statistical model of the earth's crust: Method and results. Tectonophysics **10,** Nos. 5/6 pp. 573–578

POSGAY K. 1954: On the mean error of seismic reflection measurements (In Hungarian). Geoph. Trans. **3,** No. 4, pp. 1–14

POWELL C. A., MELTZER A. S. 1984: Scattering of P-waves beneath SCARLET in Southern California. Geoph. Res. Letts. **11,** 5, pp. 481–484

RISTOW D., JURCZYK D. 1975: Vibroseis deconvolution. Geoph. Prosp., **23,** 2, pp. 363–379

ROBINSON E. A., TREITEL S. 1965: Dispersive digital filters. Rev. Geoph. **3,** No 4, pp. 433–461

ROTHROCK D. A., THORNDIKE A. S. 1980: Geometric properties of the underside of sea ice. Journal Geoph. Res. **85,** C7, pp. 3955–3963

ROTHROCK D. A., THORNDIKE A. S. 1984: Measuring the sea ice floe size distribution. Journal Geoph. Res. **89,** C4, pp. 6477–6486

RUELLE D. 1983: Five turbulent problems. Physica **7D,** Nos 1–3, pp. 40–44

STELL G. 1983: Models of disordered media: some new results including some new connections between composite-media, fluid-state, and random-flight theories. In: The mathematics and physics of disordered media. (Eds. B. D. HUGHES and B. W. NINHAM). Springer, Berlin–Heidelberg–New York–Tokyo, pp. 347–369

STEPHEN M. J. 1983: Waves in disordered media. In: The mathematics and physics of disordered media. (Eds. B. D. HUGHES and B. W. NINHAM). Springer, Berlin–Heidelberg–New York–Tokyo, pp. 400–413

STRICK F. 1971: An explanation of observed time discrepancies between continuous and conventional well velocity surveys. Geophysics, **36,** No 2, pp. 285–295

SULEM P. L., FRISCH V. 1972: Total reflection of a plane wave by a semi-infinite random medium. J. Plasma Phys. **8,** part 2, pp. 217–219

SULEM P. L. 1973: Total reflection of a plane wave from a semi-infinite, one-dimensional random medium: distribution of the phase. Physica, **70,** pp. 190–208

SZÉNÁS GY., ÁDÁM O. 1953: Seismogeological conditions in SW Hungary (In Hungarian). Geoph. Trans., **2**, 9, pp. 73–89

TEGLAND E. R. 1970: Sand–shale ratio determination from seismic interval velocity. 23rd Ann. Midwestern Mtg., SEG, AAPG, Dallas

TREITEL S., ROBINSON E. A. 1966: Seismic wave propagation in layered media in terms of communication theory. Geophysics, **31**, No. 1, pp. 17–32

TSAI C. J. 1984: An analysis leading to the reduction of scattered noise on deep marine seismic records. Geophysics, **49**, 1, pp. 17–26

VOSKRESENSKIY YU. N. 1962: A three-dimensional model study of seismic wave reflection from non-mirrorlike boundaries (In Russian). Izv. AN SSSR Ser. Geof., No 5, pp. 620–629

WATERMAN P. C.,S., TRUELL R. 1961: Multiple scattering of waves. J. Math. Phys., **2**, 4, pp. 512–537

WYLLIE M. R. J., GREGORY A. R., GARDNER L. W. 1956: Elastic wave velocities in heterogeneous and porous media. Geophysics, **21**, 1, pp. 41–70

ZIMAN J. M. 1979: Models of Disorder. The theoretical physics of homogeneously disordered systems. Cambridge University Press, Cambridge–London–New York–Melbourne

AZ ALKALMAZOTT GEOFIZIKA NÉHÁNY MEGOLDATLAN PROBLÉMÁJA

KORVIN Gábor

A cikkben nyolc megoldatlan problémát tárgyal a szerző, amelyek a statisztikus geofizikából, vagy a kőzetfizikából származnak. A problémák a következők: folyadékkal telített üledékes kőzetek effektív fizikai paramétereinek számítása *(1. és 2. probléma)*; hanghullámok abszorpciós koefficiensének függősége a heterogén kőzetek véletlenszerűségétől *(3. és 4. probléma)*; véletlenszerű közegen áthaladó jel jellemzőinek ingadozása *(5. probléma)*; véletlenszerűen disszipatív féltérről visszaverődő energia számítása *(6. probléma)*; és a véletlenszerűen egyenetlen határfelületekről visszaszórt szeizmikus jelek statisztikai tulajdonságai *(7. és 8. probléma)*. Minden esetben közli a leglényegesebb irodalmi hivatkozásokat és rámutat az alkalmazási területre.

НЕКОТОРЫЕ НЕРЕШЕННЫЕ ПРОБЛЕМЫ ПРИКЛАДНОЙ ГЕОФИЗИКИ

Габор КОРВИН

В статье автор обсуждает восемь нерешенных проблем, которые вытекают из статистической геофизики или из физики пород. Это следующие проблемы: вычисление эффективных физических параметров осадочных пород насыщенных жидкостью *(проблемы 1 и 2)*; зависимость коэффициента абсорбции звуковых волн от случайности гетерогенных пород *(проблемы 3 и 4)*; изменение параметров сигнала, проходящего через случайную среду *(проблема 5)*; вычисление отраженной энергии от случайно диссипативного полупространства *(проблема 6)*; статистические свойства отраженных сейсмических сигналов от случайно негладких поверхностей раздела *(проблемы 7 и 8)*. Автор в всех случаях дает самые важные ссылки на литературу и указывает области применения.

GEOPHYSICAL TRANSACTIONS 1985
Vol. 31. No. 4. pp. 391–403

FREQUENCY CONTENT OF SEISMIC WAVES AS A FUNCTION OF CHARGE

Hans RISCHE*

In test-measurements aimed at determining the influence of charge quantity on the frequency content of seismic waves the known relation $A = kQ^p$ was checked and improved to $p = a - b \cdot$ frequency. This relation is an adequate approximation for describing the depedence of the spectral amplitude behaviour on the quantity of charge.

Keywords: reflection method, shot-generation, charge quantity, frequency content, field tests

1. Introduction

It is well known that, in onshore seismic work, shot generation creates the best conditions for extending the effective frequency band of the seismic waves in the direction of the higher frequencies (high-frequency seismics). This extension is necessary in order to meet one of the most important requirements of geological exploration – better horizontal and vertical resolution. It can already give quite remarkable results in the presence of excellent excitation, propagation and reception conditions, and in cases where suitable generation and reception techniques are used [FARR 1976].

The essential parameters for shooting are the quantity and the depth of the charge (bearing in mind the properties of the rock close to the surface). While the depth of the charge in high-frequency work is necessarily below the low-velocity layer or in the solid rock, the only requirement for the quantity of charge is that it should be as small as possible.

Similar requirements on the quantity of the charge result when seismic waves are generated at very shallow depths [RISCHE 1985]. This technique is used particularly in cases where there is a cost limit on field work. The shooting then takes place for the most part only a few metres below ground level in the low-velocity layer. Here again the quantity of charge must be small for the technique to be successful, as has been shown by examples in exploration practice [GAERTNER et al. 1985].

* Karl-Marx-Universität, Sektion Physik, Talstr. 35, 7010 Leipzig, GDR
Manuscript received: 28 March, 1985

2. Known relations

From theoretical considerations it follows for longitudinal body waves that

$$\text{amplitude, } A = k_1 Q^{1/3}$$
$$\text{period, } T = k_2 Q^{1/3}$$
$$\text{dominant frequency, } f_0 = k_3 Q^{-1/3}$$

(Q = quantity of charge, k_1 = material-dependent factors).
Considering plane compressional waves, on the other hand, it follows that

$$A = kQ^{1/2}$$

In most cases, these relations provide the only basis for influencing the frequency content of seismic waves using the quantity of charge [ZIOLKOWSKI and LERWILL 1979].

When a charge/amplitude relation is empirically determined the result is

$$A = kQ^p$$

where p can have quite different values. According to MEISSNER and STEGENA [1979], for example, the range for p may be

$$0.5 < p < 1.3.$$

Too little is known as yet about the way in which p depends on the specific shot conditions, and no formulation exists so far.

The data published for p so far indicate that this exponent should depend also on the quantity of the charge, Q. Thus LEVYANT [1964] reported experimental results and determined

$$p = 0.85 \text{ for } 0.4 < Q < 2.5 \text{ kg},$$
$$p = 0.55 \text{ for } 2.5 < Q < 10 \text{ kg}.$$

Fig. 1 shows the values found.

Similar findings have been reported for the apparent frequency, f_0, but less experimentation has been done to verify these. What is mostly found is

$$f_0 = KQ^{-1/3} \ldots\ldots\ldots KQ^{-1/2}$$

where the exponent $-1/3$ is derived from theoretical considerations whereas $-1/2$ is derived from experimental data. Since a considerable range of scattering exists for the charge/amplitude relation whose dependence on the shot conditions is largely unknown, a situation which is at least of similar uncertainty

must be assumed for a charge/frequency relation. However, too few experimental results have been published so far for a quantitative determination of the range of this exponent.

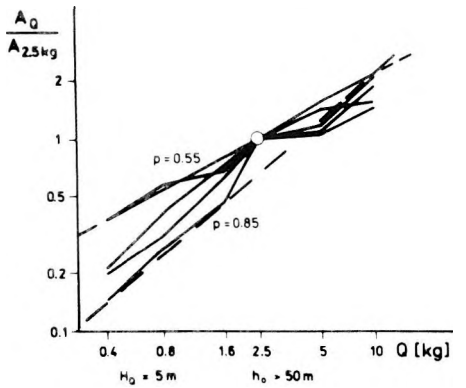

Fig. 1. Total amplitude of seismic waves as a function of charge quantity, Q [after LEVYANT 1964]. H_q – charge depth; h_o – thickness of low-velocity layer

1. ábra. A szeizmikus hullámok amplitúdója a Q töltetnagyság függvényében [LEVYANT 1964 után]. H_Q – töltetmélység; h_o – lazaréteg vastagsága

Рис. 1. Амплитуды сейсмических волн в зависимости от величины заряда Q [по Левянту 1964].
H_q – глубина заряда; h_o – мощность зоны малых скоростей

3. Graphic representation of the frequency effect

There is no prospect of solving the problem by determining the apparent frequency, f_0, with the aim of establishing a more detailed connection with the quantity of charge. The reason is that while the apparent frequency is of interest for the purpose of wave correlation and interpretation, there should be different changes caused in the specific frequency components by varying the quantity of the charge, and these can therefore be demonstrated only in the amplitude–frequency spectrum. An example of this is shown in *Fig. 2.* A good survey results from the direct comparison of spectra for various distances from the shotpoint and for individual time windows which contain different waves. It is obvious that the higher frequency portions increase as the quantity of the charge is reduced. It is conspicuous especially for the reflected waves that while the maxima change their amplitude systematically, their frequency remains stable. This applies, however, only to one reception range (x, t) each where the geophones, ground coupling, wave paths and reflection effects remained unchanged throughout the series of experiments. When, however, a comparison is made of the spectra of the reflected waves in the two different reception ranges, the position and form of the individual maxima will be found to differ

considerably. This suggests the need for a representation or calculating technique from which these effects which have been caused by wave propagation and reception, are eliminated.

Normalized spectra are compared in Fig. 2; absolute spectra are shown in *Fig. 3* that refer to the same (x, t) range as those in the centre column in Fig. 2. It is clearly demonstrated that the decrease in the amplitudes intensifies toward the higher frequencies as the quantity of charge grows, whereas it is hardly present in the frequency interval covered for which the charges are very small (e.g. two caps). The idea which suggests itself first is to try and generalize this amplitude change in the form of a simple envelope curve. It is not practical, however, because the effects from wave propagation and reception are still too strong.

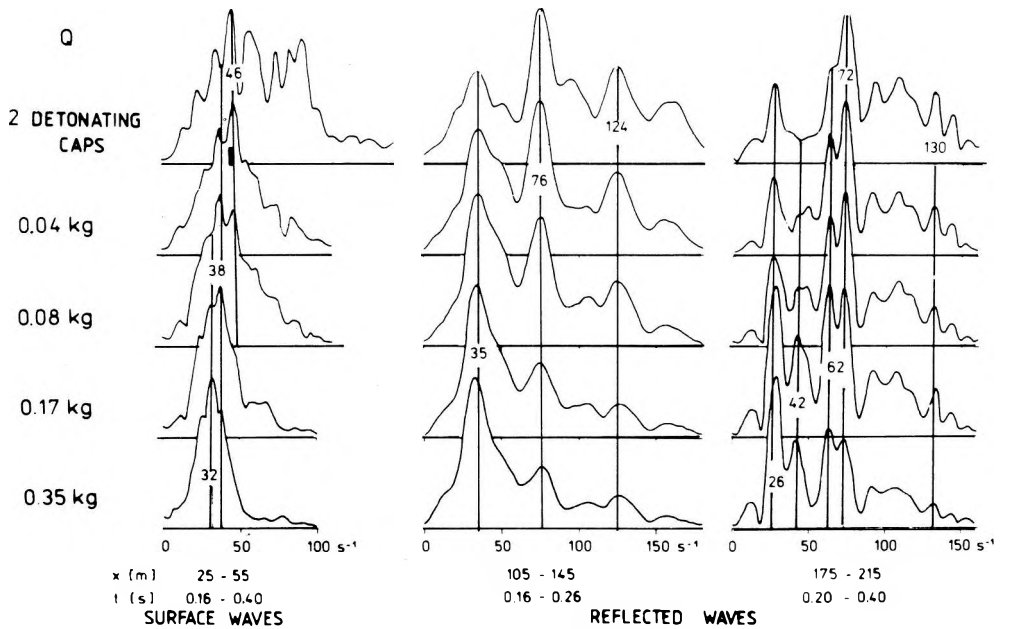

Fig. 2. Amplitude–frequency spectra for variations of charge quantity, Q, and for different distances x from the shot point and different time intervals Δt. Charge depth: 15 m, closely below low-velocity layer

2. ábra. Amplitúdó–frekvencia spektrumok változó Q töltetnagyságra és különböző x robbantópont távolságokra, különböző Δt időablakokban. Töltetmélység: 15 m, közvetlenül a lazaréteg talpa alatt

Рис. 2. Амплитуды–частотные спектры при разных величинах заряда Q и расстояний между пунктом взрыва и пунктом приема в разных временных окнах. Глубина заряда 15 м, непосредственно под зоной малых скоростей

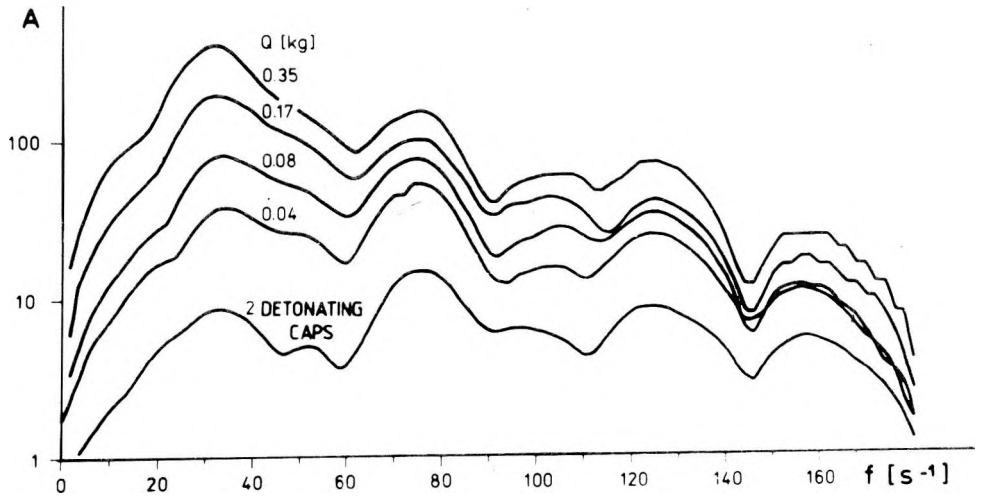

Fig. 3. Absolute amplitude spectra for different charge quantities, Q (for data, see Fig. 2, centre column)

3. ábra. Különböző Q töltetnagyságokhoz tartozó abszolút amplitúdóspektrumok (adatok, mint a 2. ábra középső oszlopában)

Рис. 3. Абсолютные амплитудные спектры, относящиеся в разным величинам заряда Q (данные также как в среднем столбце, рис. 2)

As a next step one may try to show the spectral amplitude response separately for the individual frequency components as a function of the quantity of the charge. *Fig. 4* indicates that this appears to be a good approach to quantifying the relation between the quantity of the charge and the frequency. At low frequencies the amplitudes increase with the quantity of the charge and then decrease from about 30 Hz onward. This decrease is greatest at about 40 Hz and then diminishes with increasing frequency. There is the same trend for all three reception ranges analysed, with regard both to surface waves and reflected waves, and the predominant effect of wave propagation and reception has been eliminated.

When one changes over now to the amplitudes of the absolute spectra and selects a double logarithmic scale, a type of representation results which was once tried by MOLOTOVA [1964] but has not been used since *(Fig. 5)*. It can provide p values for each frequency interval and each individual frequency component, which then serve as a measure of changes in the spectral amplitude portion as a function of the quantity of the charge. When the p values found in this manner are summarized as a function of frequency, this should give a suitable approach to determining charge quantity–frequency relations. This should make it possible to compare quantitatively the different excitation conditions such as the depth of the charge, the surrounding rock and the type of explosive.

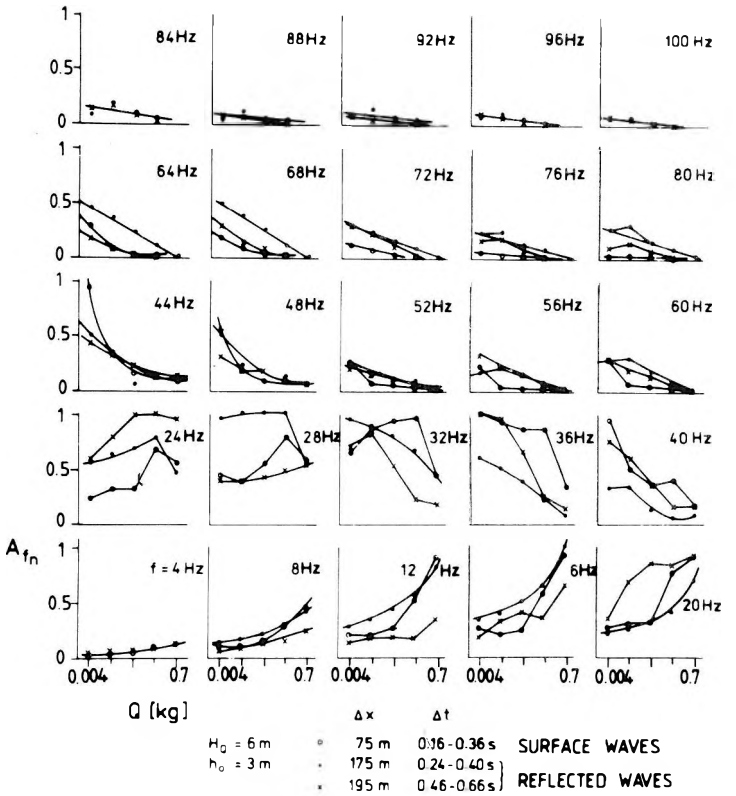

Fig. 4. Amplitudes of normalized spectra as a function of charge quantity, Q, for individual frequency components (for data see Fig. 2)
H_Q – charge depth; h_o – thickness of low-velocity layer

4. ábra. Normált amplitúdóspektrumok a Q töltetnagyság függvényében, kiválasztott frekvencia komponensekre. H_Q – töltetmélység; h_o – lazaréteg vastagsága (adatok, mint a 2. ábrán)

Рис. 4. Нормализованные амплитудные спектры на выбранные компоненты частот в зависимости от величины заряда.
H_Q – глубина заряда; h_o – мощность зоны малых скоростей (данные также как в рис. 2)

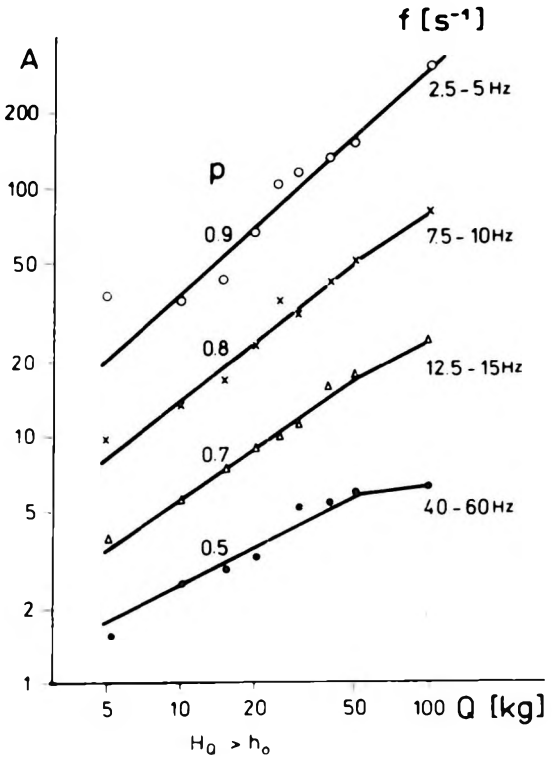

Fig. 5. Amplitudes of seismic waves as a function of charge quantity, Q, for different frequency intervals [after MOLOTOVA 1964].
H_Q – charge depth; h_o – thickness of low-velocity layer

5. ábra. A szeizmikus hullámok amplitúdói a Q töltetnagyság függvényében, különböző frekvencia-intervallumokban [MOLOTOVA 1964 után]
H_Q – töltetmélység; h_o – lazaréteg vastagsága

Рис. 5. Амплитуды сейсмических волн в разных частотных интервалах в зависимости от величины заряда [по МОЛОТОВОЙ 1964].
H_Q – глубина заряда; h_o – мощность зоны малых скоростей

4. A graphical-numerical method

In a relation

$$A(Q, f) = kQ^{p(f)}$$

or

$$\lg A_{f_i}(Q) = \lg k + (\lg Q)\,(p_{f_i})$$

the following applies to each frequency component of the spectrum:

$$p_{f_i} = \frac{\lg A_{f_i, Q_2} - \lg A_{f_i, Q_1}}{lg\, Q_2 - lg\, Q_1}$$

In this way the p_{f_i} values can be determined from the inclination of straight lines. For a sufficiently safe determination of the inclination of the straight line it is useful to have readings available for several (at least four) different charge quantities. The individual charges in a series of experiments should differ by a factor of two each. Figs. 6–8 demonstrate how such a series of experiments is evaluated.

Fig. 6 shows the spectral amplitudes derived from the absolute amplitude spectra, as a function of the quantity of the charge. As can be seen, the relevant readings can be summarized to give straight lines. The p_{f_i} determined from these are plotted on the r.h. side of Fig. 6. From this series of data it is already clear that a systematic connection should exist between p and f.

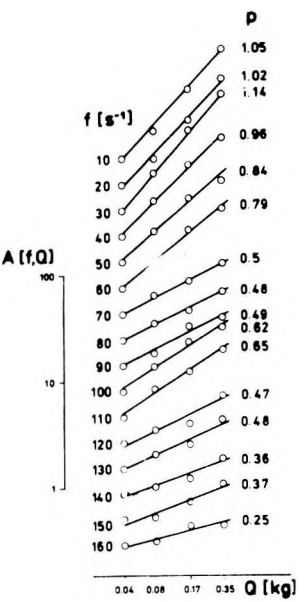

Fig. 6. Spectral amplitudes of reflected waves as a function of charge quantity for determining exponent p (for data, see Fig. 2, centre column)

6. ábra. Reflektált hullámok spektrum-amplitúdói a töltetnagyság függvényében a p kitevő meghatározására (adatok, mint a 2. ábra középső oszlopában)

Рис. 6. Спектральные амплитуды отраженных волн, в зависимости от величины заряда для определения показателя «p». (Данные также как в среднем столбце рис. 2)

When these p_{f_i} values are plotted against the frequency, the result provides the desired quantitative relation. For example, *Fig. 7* summarizes the p values of Fig. 6. The reduction of p with increasing frequency which has been previously detected in a qualitative sense, is now quite obvious. Now the attempt can be made to determine an approximate function, in this case a straight line

$$p = a - bf$$

where the constants a and b are the desired comparative values which indicate the change in the spectral amplitudes when the quantity of the charge varies (f denotes frequency). The only remaining effects on these constants are essentially the surrounding rock and the depth of the charge.

This statement must, however, be qualified in one respect. As has been said, some workers report that the exponent p in the relation $A = kQ^p$ is dependent also on the quantity of the charge in cases where the charge quantity interval under consideration is quite large (see for example Fig. 1). In these cases p is reduced as the quantity of the charge increases. It therefore appears desirable to define the p values obtained and/or the function $p = f$ (frequency) with its constants determined from these values, only for a specific range of charge quantities that should not be too wide.

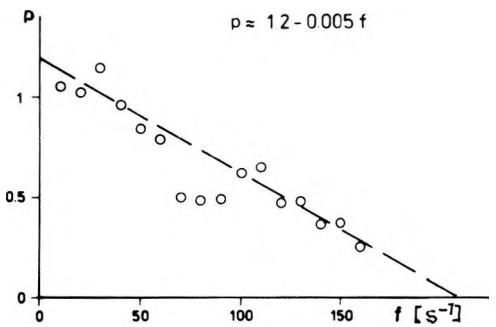

Fig. 7. Exponent p as a function of frequency (values from Fig. 6)

7. ábra. A p kitevő a frekvencia függvényében (a 6. ábráról vett adatok)

Рис. 7. Показатель «p» в зависимости от частот (данные взяты из рис. 6.)

Fig. 8 is intended as an illustration of the fact that the determination of p may be rather difficult. It shows the values for the surface waves from Fig. 2, and there is an obvious difference between these and the reflected waves (Fig. 6). The amplitude curve inclinations can be determined only up to 40 Hz because no straight lines can be formed beyond 50 Hz. In these cases it will not be possible, for the time being, to identify p and, as a result, $p = f$ (frequency). Instead the representation $\lg A = F(\lg Q)$ must be used for assessment and comparison. In this example, reflected waves may possibly have an effect on the data, considering the low charge quantities.

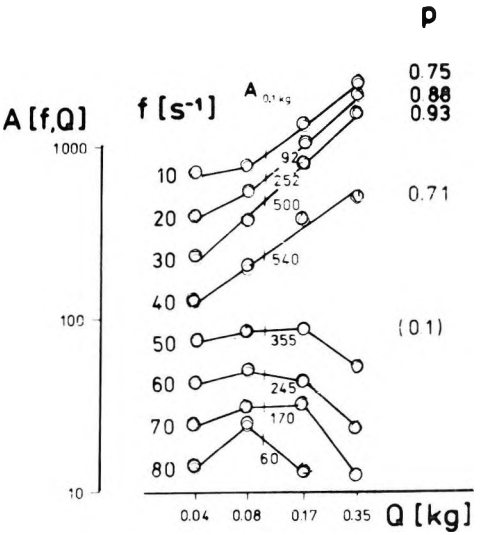

Fig. 8. Spectral amplitudes of surface waves as a function of charge quantity for determining exponent p (for data, see Fig. 2, left column)

8. ábra. Felületi hullámok spektrum-amplitúdói a töltetnagyság függvényében a p kitevő meghatározására (adatok, mint a 2. ábra baloldali oszlopában)

Рис. 8. Спектральные амплитуды поверхностных волн, в зависимости от величины заряда для определения показателя «p». (Данные также как в левом столбце рис. 2)

Finally, mention should be made of another possibility for determining p which can be used when readings are available for only two different charge quantities. An alternative to

$$p_{f_i} = \frac{\lg A_{f_i,Q_2} - \lg A_{f_i,Q_1}}{\lg Q_2 - \lg Q_1}$$

is

$$p_{f_i} = \frac{\lg (A_{Q_2}/A_{Q_1})_{f_i}}{\lg (Q_2/Q_1)}$$

where $(A_{Q_2}/A_{Q_1})_{f_i}$ (in the range $0 \leqq f_i \leqq$ maximum frequency with an amplitude which can still be evaluated) is the division of the two spectra for Q_2 and Q_1. Since $\lg (Q_2/Q_1)$ is constant here, p can be determined from the spectral division. One should, however, be careful of this kind of determination because the accidental effect from a single shot which is reduced by the formation of straight lines in the event of several charges, may excessively influence the result. An example of this type of determination is given in *Fig. 9*. Here it seems just about

possible to eliminate the effect of a connection between p and f (caused by a slight shift in the amplitude maxima of the two spectra), particularly for the higher frequencies. As for the low frequencies, however, the shape of a curve already becomes quite problematic.

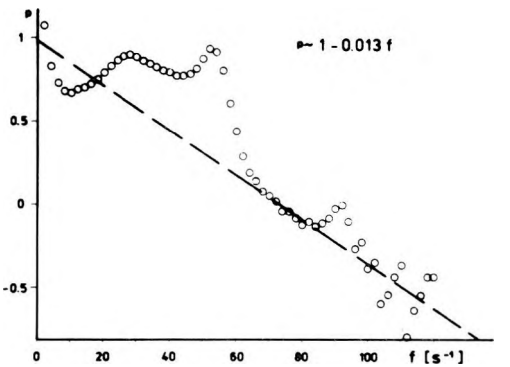

Fig. 9. Exponent p as a function of frequency, determined from spectral division for two charge quantities ($Q_2 = 0.17$ kg, $Q_1 = 0.04$ kg)

9. ábra. A p kitevő a frekvencia függvényében, két töltetnagysághoz tartozó spektrum hányadosából meghatározva ($Q_2 = 0{,}17$ kg, $Q_1 = 0{,}04$ kg)

Рис. 9. Показатель «p» в зависимости от частоты, определяемый делением спектров, относящихся к двум величинам заряда ($Q_2 = 0{,}17$ кг, $Q_1 = 0{,}04$ кг)

5. Preliminary results

The following data have so far resulted from an analysis of charge quantity tests for the Cenozoic:

Area	Q(kg)	H_Q(m)	h_0(m)	Wave type	a	b
1	0.04 – 0.35	15	14	reflected	1.2 1.15	0.005 0.005
		5	14	reflected	1.0 1.1	0.013 0.01
2	0.04 – 0.7	18	15	reflected	1.25	0.004
		6	15	reflected surface wave	1.7 2.3 1.8	0.008 0.027 0.023
3	0.04 – 0.17	24	21.5	reflected	1.7	0.01
		6	21.5	reflected	2.0	0.016

This makes it possible to estimate quantitatively the effect of the charge quantity on the frequency content of seismic waves for an area studied and under the measuring conditions selected. For example, the following can be concluded for area 1:

The constants a and b are

for shooting below the low-velocity layer (LVL) $a=1$, $b=0.005$

for shooting in the low-velocity layer $a=1$, $b=0.01$.

From this it follows for shooting	in the LVL	below the LVL
$A \sim Q^1$ for frequencies around	0– 20 Hz	0– 40 Hz
$A \sim Q^{1/2}$	40– 60 Hz	80–120 Hz
$A \sim Q^0 = \text{const.}$	80–120 Hz	180–220 Hz
$A \sim Q^{-1/2}$	150 Hz	300 Hz

This means that in the case of shooting in the low-velocity layer any growth of the charge quantity in the normalized amplitude spectrum causes a reduction of the higher frequency portions which is double that for shooting below the LVL. Or, conversely, any reduction of the charge quantity will roughly raise the higher frequencies in the normalized amplitude spectrum twice as much if the charge is exploded immediately in the low-velocity layer, compared with an explosion below the LVL. The decisive factor for the measuring quality and for approaching geological projects in these cases therefore consists of finding a charge quantity which is just about sufficient.

6. Concluding remarks

In the three areas studied, the relation $p = a - bf$ (see table) which has been obtained is an adequate approximation for describing the dependence of the spectral amplitude behaviour on the quantity of the charge. In area 3 it is suggested that this dependence can also be expressed by the relation $p = a - bf^q$ $(1 < q < 2)$. This is why the results presented here are intended only as examples whose applicability is restricted to the particular area being studied. Regardless of the type of this relation, however, the determination method used, and the quantifiable statement in comparing different excitation parameters, are generally practicable.

REFERENCES

Farr J. B. 1976: Very high resolution seismic profiling. 38th EAEG Meeting, The Hague, Preprint

Gaertner H., Rische H., Fischer K. H. 1985: Schusseismische Braunkohlenerkundung als Alternativlösung. Zeitschr. f. Geol. Wissensch. **13**, 1, pp. 23–32

Levyant V. B. 1964: On the effectiveness of near-surface explosions for seismic measurements (a case history of the Volgograd area (in Russian). Geol. i razv. 10, pp. 123–140

Meissner R., Stegena L. 1977: Praxis der seismischen Feldmessung und Auswertung. Akadémiai Kiadó, Budapest

MOLOTOVA, L. V. 1964: On the influence of explosion conditions on the frequency spectra of seismic waves. I. Results of experimental measurements (in Russian). Izv. A.N. SSSR. Ser. geof., 12, pp. 1753–1766

RISCHE H. 1985: Anregung seismischer Wellen in sehr geringen Tiefen. Geophysik und Geologie, **3**, 2, pp. 125–136

ZIOLKOWSKI A., LERWILL W. E. 1979: A simple approach to high-resolution seismic profiling for coal. Geophysical Prospecting **27**, 2, pp. 360–393

SZEIZMIKUS HULLÁMOK FREKVENCIA-TARTALMÁNAK FÜGGÉSE A TÖLTETNAGYSÁGTÓL

Hans RISCHE

A töltetnagyság – frekvencia-tartalom összefüggés vizsgálatára végzett kísérleti mérések során az ismert $A = kQ^P$ összefüggést ellenőrizték és egy jobb, $p = a - b \cdot$ frekvencia kapcsolatot határoztak meg. Ez az egyenlet megfelelő pontossággal közelíti az amplitúdóspektrum töltetnagyságtól való függését.

ЗАВИСИМОСТЬ ЧАСТОТЫ СЕЙСМИЧЕСКИХ ВОЛН ОТ ВЕЛИЧИНЫ ЗАРЯДА

Ганс РИШЕ

При проведении опытных измерений с целью изучения зависимости частоты от величины заряда проверялась известная зависимость $A = kQ^P$ и определялась более точная связь: $a - bf$. Это новое уравнение достаточной точностью приближает зависимость амплитудного спектра от величины заряда.

GEOPHYSICAL TRANSACTIONS 1985
Vol. 31. No. 4. pp. 405–417

COMPUTATION AND RELIABILITY OF PSEUDO-POROSITY SECTIONS FROM SEISMIC DATA

Imre SZULYOVSZKY*

The paper compares the porosity section computed from a pseudo-acoustic impedance section with borehole data from a productive area. An investigation on the distortion in porosity computation is performed in a sand reservoir using seismic acoustic impedance instead of velocity, and the average values of other parameters.

Keywords: reflection seismics, pseudo-acoustic impedance, porosity transformation, porosity prediction, Wyllie relationship, sandstone reservoir

1. Introduction

The transformation of a seismic section into a pseudo-acoustic impedance section – using, for example, recursive inversion – opened new ways to get information that was not part of conventional seismic processing. The pseudo-acoustic impedance section was the first [LINDSETH 1979]. Its information content is the same as that of the original seismic section but the appearance is different. The amplitudes in the original seismic section are proportional to the derivative of the acoustic impedance but the amplitudes in the pseudo-acoustic impedance section are proportional to the acoustic impedance, one of the important physical parameters. The reliability of the pseudo-acoustic section may be enhanced by borehole data. The pseudo-acoustic impedance section – though with limited accuracy and much less resolving power – can be used as a series of acoustic impedance logs and, for example, a porosity section can be computed.

The reliability of the derived porosity is not as great as the reliability of the borehole porosity although the seismic porosity represents continuous information along the seismic line. The derived porosity section may be called pseudo-acoustic porosity and it approximates only acoustic porosity derived from well log data.

In order to compute the pseudo-acoustic porosity, the pseudo-acoustic impedance section is required and to compute the latter borehole information is needed. Seismic processing yields an approximation of the reflection coefficient series restricted by the seismic frequency band. It is well known that the acoustic impedance series and the reflection coefficient series represent the same

* Geophysical Exploration Company, POB 213, Budapest, H–1391, Hungary
Manuscript received (revised form): 16 May, 1985

information – they can be transformed into each other, but only if the starting velocity is known. Moreover, the seismic method has a restricted resolution. In a real case the starting velocity is not known and the seismic resolution is not large enough to gain information about the fine structure of the geological sequence. In view of this, an infinite number of real acoustic impedance functions may be ordered to a fixed seismic reflection coefficient series. Similarly, an infinite number of lithology sections may be ordered to the fixed acoustic impedance function. Porosity is a lithology parameter, consequently, starting from seismic information to get lithology information, e.g. to get porosity without borehole information, is just not possible. Velocity, fluid content and lithology must be known to obtain a correct porosity prediction. The Wyllie time average relation – the porosity transformation equation – is experimentally determined for a fixed lithological unit. In its well log application corrections are used to eliminate the distorting effects of some parameters. Acoustic porosity is only one of the components in an effective porosity determination since porosity data may be computed from gamma-gamma, neutron-gamma and resistivity logs.

When predicting porosity from seismic data the possibilities are more restricted than in the case of well log data but, by investigating the correctness of the relation, the reliability of the results can be checked. Porosity is one of the most significant parameters in a reservoir so it seems to be worth determining it from seismic data, even with limited accuracy.

2. Acoustic porosity prediction from seismic data

To compute seismic pseudo-acoustic porosity, the absolute velocity function is needed. Therefore, the first step is to obtain a reliable absolute pseudo-acoustic impedance section. In most cases relative sections are sufficient since the anomalies are recognizable. To compute a relative pseudo-acoustic impedance section, the proper seismic phase has to be used, and the approximate scaling of the seismic section and the approximate starting velocity are necessary. To compute the absolute section, the following additional information is required: the exact values of the scaling coefficient, the starting velocity and the low frequency acoustic impedance component. All of these can reliably be acquired from borehole data. The easiest way to check and find the correct values of all the above parameters is the following: a nearby borehole acoustic impedance is measured, the pseudo-acoustic impedance section is computed with the estimated parameters, and the borehole acoustic impedance log and a pseudo-acoustic impedance trace close to the borehole is displayed. All the parameters are varied to get minimum discrepancy between the two traces. The longer the borehole log, the better the parameter estimation.

Figure 1 shows part of a seismic section from a productive area. The borehole locations are shown (A and B). Their offset distance from the seismic line is 150 m on both sides. The result of the foregoing parameter estimation

is shown in *Fig 2*. A is the CDP trace close to the borehole, B is the same trace after deconvolution, C is the borehole acoustic impedance trace, D is the borehole acoustic impedance trace superimposed on the pseudo-acoustic impedance trace.

Figure 3 shows an absolute pseudo-acoustic impedance section. The acoustic-impedance log of borehole B is displayed at the nearest trace, both traces drawn in heavier lines. The coordinate system of the borehole acoustic impedance log is displayed too. If the coordinate system is shifted to any CDP point the value of the pseudo-acoustic impedance can be read at any time.

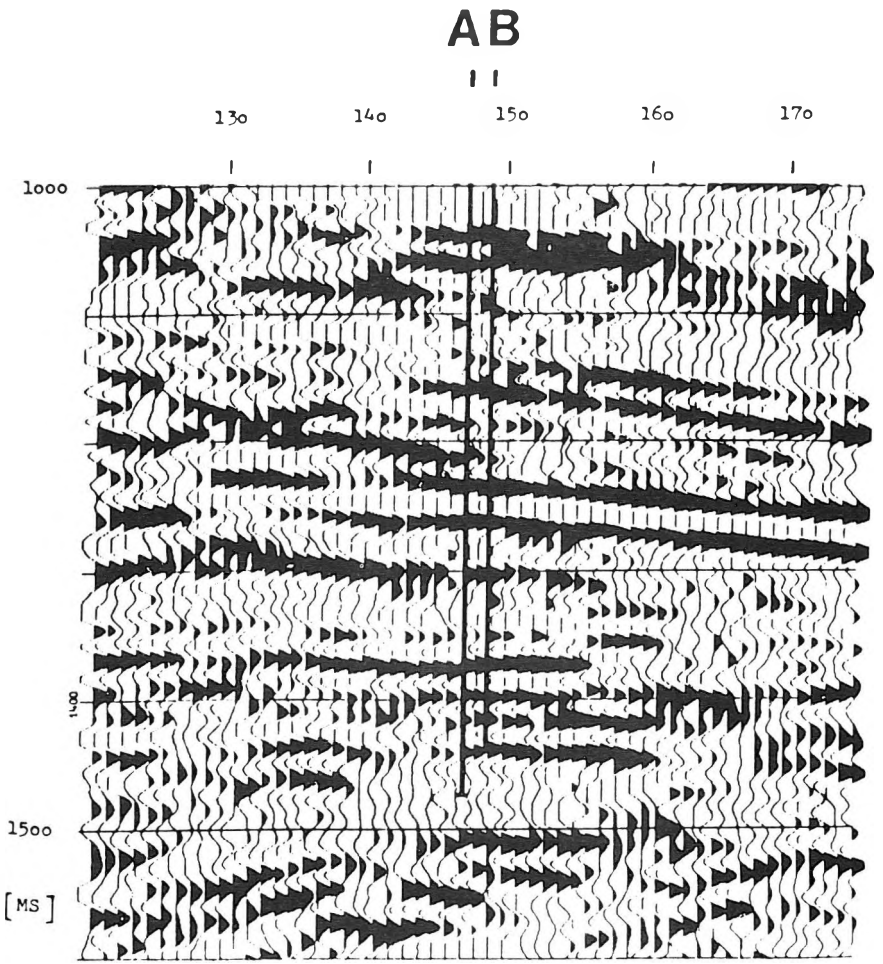

Fig. 1. Seismic time section with borehole locations A and B

1. ábra. Szeizmikus időszelvény az A és B mélyfúrás helyével

Рис. 1. Временной разрез местами глубокого бурения А и В

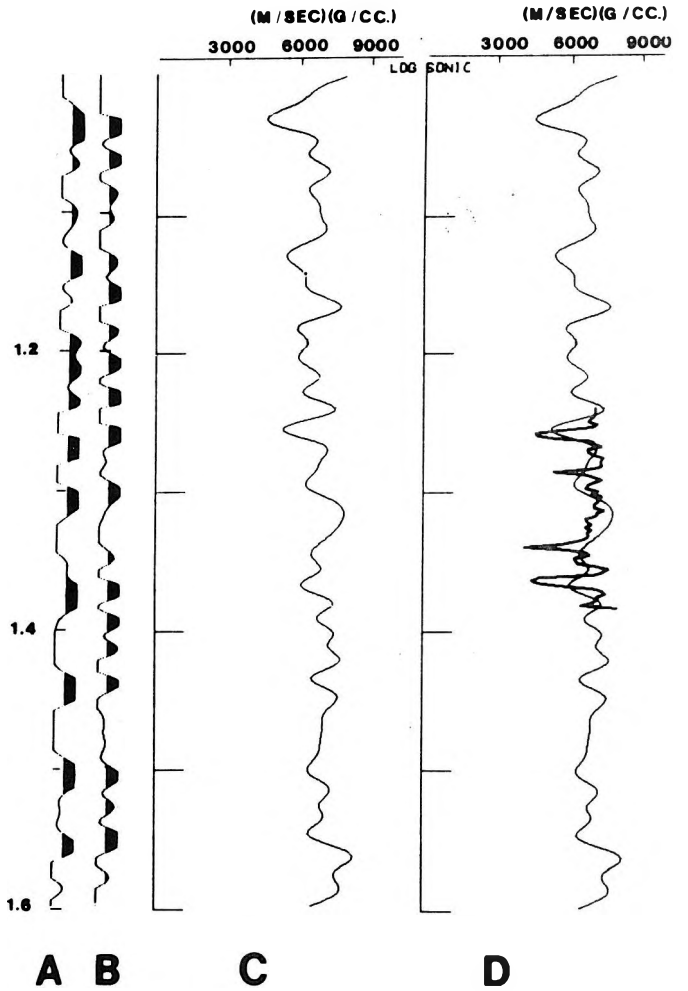

Fig. 2. Borehole acoustic impedance log and pseudo-acoustic impedance log close to the borehole. A: CDP seismic trace, B: trace A after deconvolution, C: pseudo-acoustic impedance trace computed from trace B, D: trace C and the borehole acoustic impedance log shown together

2. ábra. A mélyfúrás közelébe eső pszeudoakusztikus impedancia-szelvény és a mélyfúrási akusztikus impedancia görbe. A: szeizmikus összeg-csatorna, B: dekonvolvált összegcsatorna, C: pszeudoakusztikus impedancia csatorna B-ből számítva, D: a C csatorna és a mélyfúrási akusztikus impedancia görbe együtt

Рис. 2. Разрез псевдоакустической жесткости и кривая акустической жесткости, находящиеся вблизи глубокого бурения. A: сейсмическая суммотрасса, B: суммотрасса после деконвольции, C: трасса псевдоакустической жесткости, вычисленная из B, D: трасса C и кривая акустической жесткости вместе

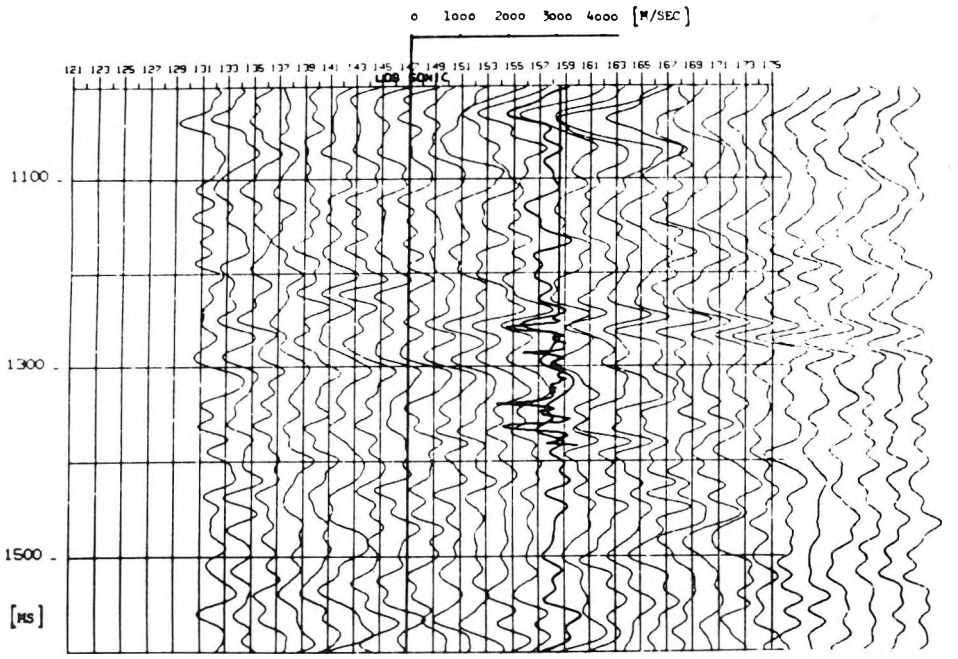

Fig. 3. Absolute pseudo-acoustic impedance section with the borehole acoustic-impedance log

3. ábra. Az abszolút pszeudoakusztikus impedancia szelvény a mélyfúrási akusztikus impedancia görbével

Рис. 3. Разрез абсолютной псевдоакустической жесткости вместе с кривой акустической жесткости

We can compute acoustic porosity from all the traces of this absolute pseudo-acoustic impedance section. The computation is made by the Wyllie time average relation. This equation supposes that the porosity is intergranular and only the rock matrix and the interstitial fluids are present. The formula including transit times is well known:

$$\Phi = \frac{\Delta t - \Delta t_{ma}}{\Delta t_f - \Delta t_{ma}}$$

where Φ denotes porosity

Δt_{ma} transit time of the rock matrix

Δt_f transit time of the interstitial fluids.

The formula was experimentally determined for brine-filled sandstones of variable porosity and in this case it is substantially accurate. In all the cases which are different from this we have to correct the distorting effects. These may be, for example, as follows:

- Low consolidation: extremely high values of porosity would be computed.
- Shale content: the transit time is higher than in the case of a rock with the same porosity but without shale content, therefore the derived porosities seem to be higher than the real values.
- Hydrocarbon content: the velocity decreases (transit time increases) in the presence of a certain percentage of gas so higher porosity values result as compared with the real values.
- Too high porosity may appear as a distorting effect when using the borehole sonic log – since in this case the invaded zone is thin, the mud cake is thick, the original pore content remains in the pores of the invaded zone. In case of gas content the resulting porosity must be multiplied by a factor of approx. 0.8.

To eliminate the above distortions empirical corrections are employed. It is clear that the computation of acoustic porosity is not without difficulties even when using well log data.

When computing the porosity from seismic data, the above mentioned distorting effects also appear – with the exception of the different invasion effects. These additional distorting effects may be as follows:

- The pseudo-acoustic impedance traces are strongly band-limited compared with the borehole sonic log.
- The pseudo-acoustic impedance trace is an approximation of the acoustic impedance log, yet the Wyllie relation uses transit times. The effect of density must be eliminated or investigated.
- A seismic trace and the pseudo-acoustic impedance trace can be seen as a composition of constructive and destructive interferences. The largest amplitude anomalies of the seismic trace are not in correlation with the largest acoustic-impedance variations in any situation. In view of this the pseudo-acoustic impedance trace cannot be expected to approximate closely the real acoustic log. Moreover, non-productive buildups can generate similar acoustic-impedance anomalies as a porosity anomaly but in the procedure it is handled as a porosity anomaly.
- We are not able to change lithology parameters from sample to sample as in borehole data processing, since these are not available for the whole seismic section.
- 5% relative error in transit time causes about 16% relative error in the resulting porosity at $\Phi = 20\%$ porosity value. Obviously, the transit times computed from the seismic section are not precise so the seismic acoustic porosity values are somewhat qualitative in nature.

In practice it is indispensable to examine the measure of the different distorting effects. The following analysis was made on the borehole data of the investigated area. We have checked the sandstones in the area to ascertain its state of consolidation. *Figure 4* shows the relation of density and velocity in borehole A. We used the logarithm of the density and velocity; the circles show sands, asterisks show shales. We made linear regression for sands, for shales and

also for the whole data set. The relation between the density and velocity – after GARDNER et al. [1974] – is given by

$$\varrho = Av^B$$

where $A = 0.31$, $B = 0.25$, for depositions, when the velocity is measured in m/s, the density in g/cm^3.

The parameters of the regressions are as follows:

sandstones	$A = 0.13$	$B = 0.35$	$C = 0.78$
shales	$A = 0.35$	$B = 0.24$	$C = 0.77$
whole data set	$A = 0.42$	$B = 0.22$	$C = 0.65$

where C is the correlation coefficient.

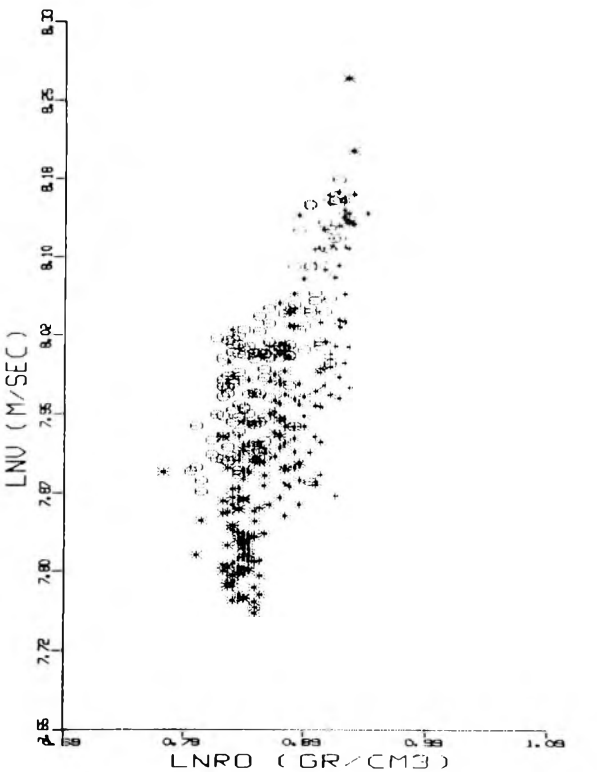

Fig. 4. Velocity – density relation

4. ábra. Sebesség – sűrűség összefüggés

Рис. 4. Зависимость между скоростью и плотностью

We see from the figure and from the regression coefficients that the sands and shales are well separated by density and velocity values: the correlation coefficient is much better for the separated data than for the whole data set. The coefficients are near to the published values. The average velocity for sands is about 3050 m/s [328 μs/m] which corresponds to consolidated sandstone.

The Wyllie formula requires transit times; from the pseudo-acoustic impedance we get acoustic impedance values. There is some possibility to compensate the effect of density: by interpolation, extrapolation of well log data, or by establishing a statistical relation as before but it is not mandatory to apply the correction. In cases when the seismic dynamics is governed by density variations [GOGONENKOV–KRASAVIN 1983] the correction must be carried out otherwise it is nonsensical to compute seismic porosity because the reliability will be very poor.

If the seismic dynamics is governed by velocity variations, the reliability of the resulted seismic porosity will be better but the effectiveness of the density correction must be verified to avoid generating larger errors with the correction. *Figure 5* shows the density, the velocity and the acoustic impedance curves in borehole A. The acoustic impedance curve is very similar to the velocity curve so, using constant density, we can compensate the effect of density in an acceptable way. If we have core samples, additional investigations may be made.

When the above investigations show a good correlation between borehole acoustic porosity and seismic pseudo-acoustic porosity, there are two ways to get the porosity section from the seismic section. The first is to transform the pseudo-acoustic impedance traces to a porosity section, using the borehole data, making the empirical corrections as mentioned on page 410, comparing the nearest corrected trace with the effective porosity resulting from integrated well log interpretation and – thus calibrating the seismic porosity trace. The other way is stratigraphic interpretation, average transit time determination and porosity computation for the strata [ANGELERI–CARPI 1982, MAUREAU–VAN WIJHE 1979].

We have followed the first option. The determination of the lithology parameters was done in the following way: Fig. 4 shows that the average velocity of the sandstone is about 3050 m/s [328 μs/m]; the average velocity of the shales is about 2750 m/s [364 μs/m]. This sandstone velocity is in the lower part of the customary consolidated sandstone velocity range. This shale velocity is higher than the customary shale velocity range. In addition, it overlaps the velocity range of the consolidated sandstones. The reason for this is probably that they are not clean formations; the sand has an average 23% shale, shale has an average of 15% sand content so the velocities are close. Consequently, the whole section can be handled as a homogeneous formation in view of porosity. Since the sandstones can be regarded as consolidated sandstones, we have used a transit time of 180 μs/m for the matrix.

For fluid transit time we have used the recommended 620 μs/m value; 23% average shale content was used during the transformation. *Figure 6* shows the derived porosity section. Its reliability can be checked in the same manner as

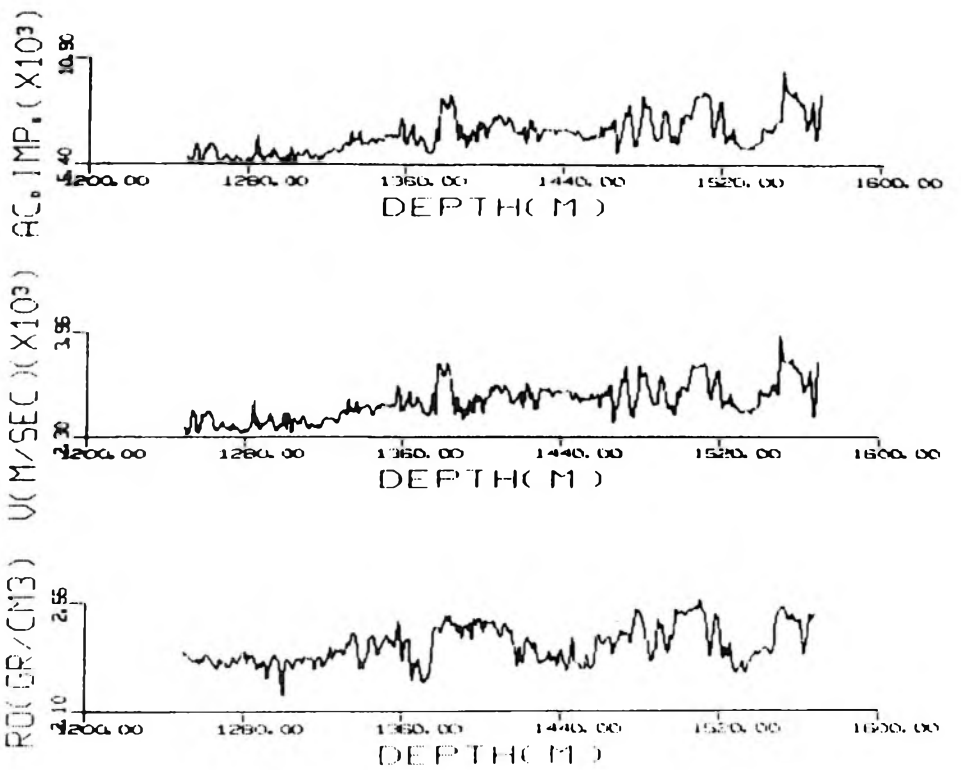

Fig. 5. Borehole density, velocity and acoustic impedance logs

5. ábra. Mélyfúrási sűrűség-, sebesség- és akusztikus impedancia görbe

Рис. 5. Кривые плотности, скорости и акустической жесткости, полученной при глубоком бурении

in the case of the pseudo-acoustic impedance computation. The well data from borehole B and a nearby seismic porosity trace are shown in *Figure 7*. Trace I is SW: water saturation; SXO: the flushed zone water saturation; SWR: residual water saturation. The dark zones mark the gas-bearing layers. Trace II is the effective porosity result of well log interpretation; trace III is the acoustic porosity computed from the sonic log; trace IV is the porosity computed from the well acoustic impedance data. No essential difference is present between the porosity logs computed from sonic or acoustic impedance trace. The gas-bearing layers appear with strong anomalies for which – applying the correction – the porosity values are acceptable. The last trace (V) is the nearby seismic porosity trace. This shows quite good agreement with the well log acoustic porosity trace, if smoothed as if filtered in the seismic band-pass.

The layers between 1440–1480 m have rather high porosity and they contain water judging by other well logs. This is not seen in the borehole

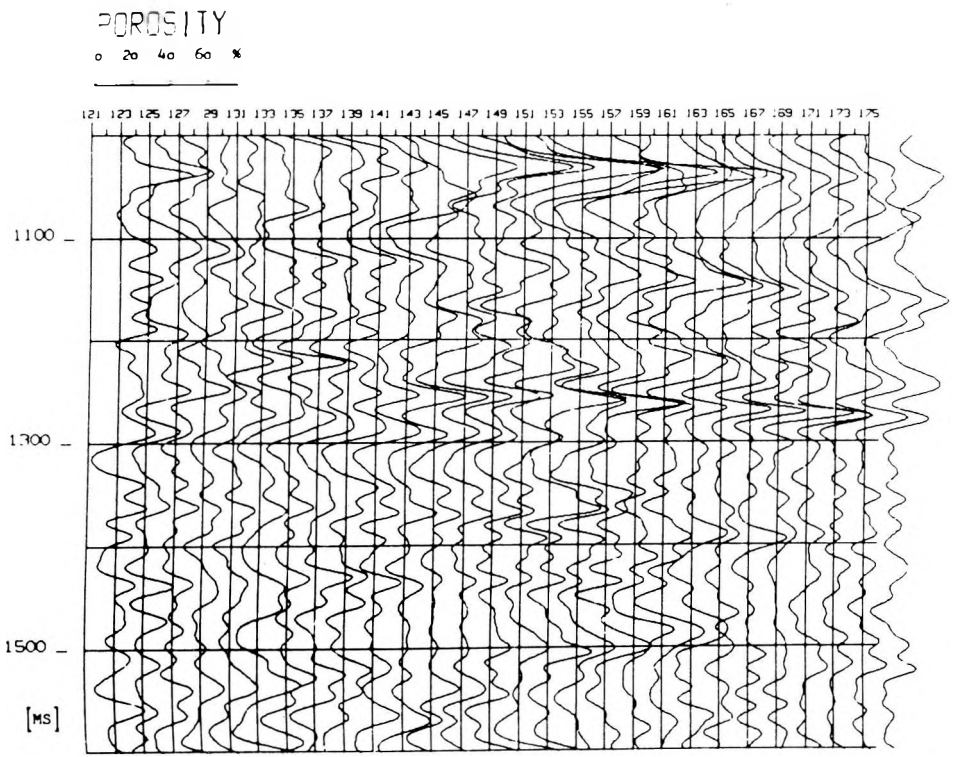

Fig. 6. Porosity section

6. ábra. Porozitás szelvény

Рис. 6. Разрез пористости

7. ábra. Mélyfúrási információk és a szeizmikus porozitás csatorna
I: SW – víztelítettség, SXO – elárasztott zóna víztelítettsége, SWR – maradék víztelítettség; II: effektív porozitás a karotázs görbék komplex értelmezéséből; III: akusztikus porozitás, az akusztikus karotázsból számítva; IV: porozitás, az akusztikus impedancia adatokból számítva; V: szeizmikus porozitás csatorna

Рис. 7. Данные глубокого бурения и сейсмическая трасса пористости
I: SW – водонасыщенность; SXO – водонасыщенность замытой зоны, SWR – остаточная водонасыщенность; II: эффективная пористость полученная по комплексной интерпретации каротажных кривых; III: акустическая пористость, вычисленная из данных акустического каротажа; IV: пористость, вычисленная из данных акустической жесткости V: сейсмическая трасса пористости

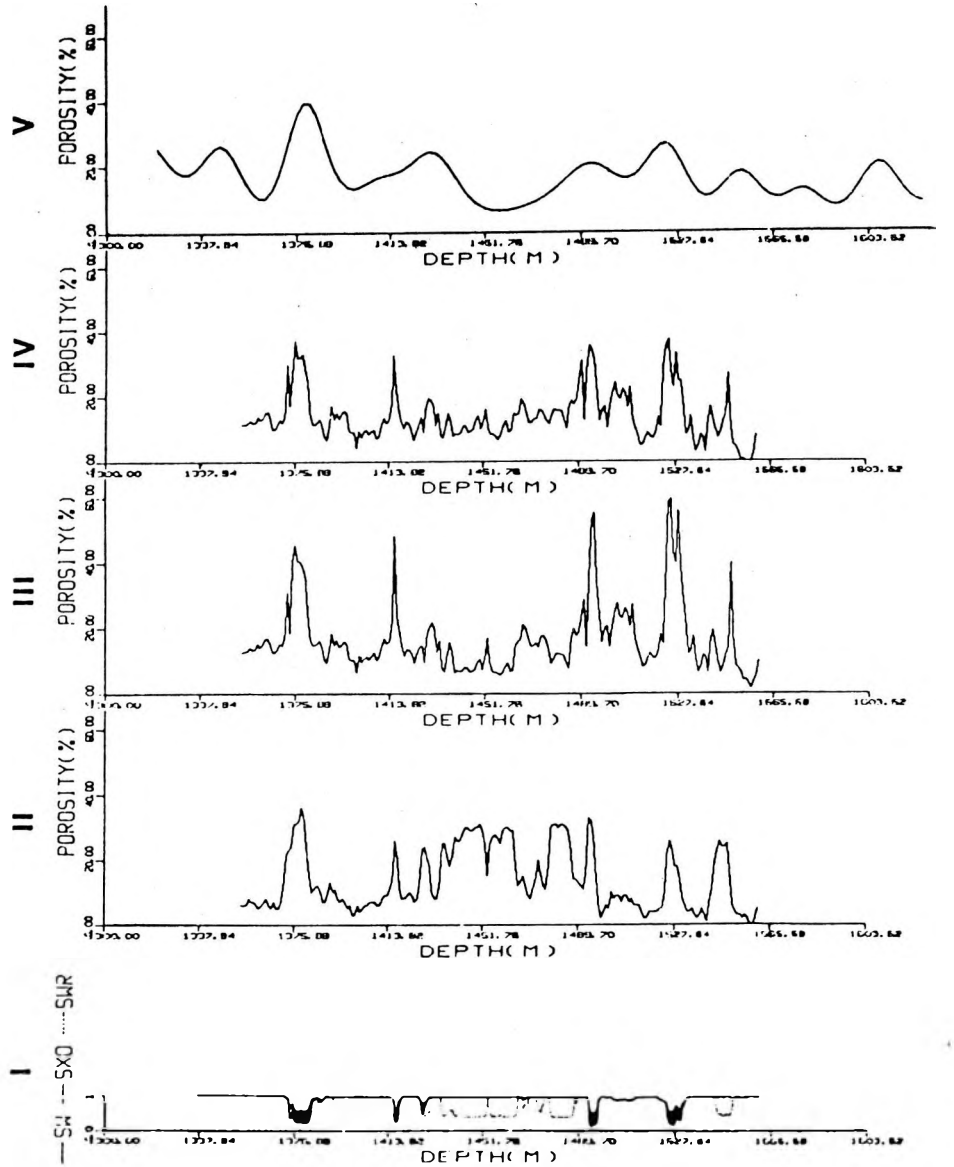

Fig. 7. Borehole information and seismic porosity trace
I: SW – water saturation, SXO – flushed zone water saturation, SWR – residual water saturation; II: effective porosity from integrated well log interpretation; III: acoustic porosity computed from sonic log; IV: porosity computed from acoustic impedance data; V: seismic porosity trace

acoustic porosity nor in the seismic acoustic porosity. To trace these layers the corrections would have to be carried out more exactly, resulting in more detailed well acoustic porosity values. In seismic application we have carried out the corrections only in smoothed form in agreement with the seismic resolving power which is far smaller than that of the well log resolving power. In spite of this limitation the gas-bearing layers appear with good detectable porosity maxima in the seismic porosity trace too.

3. Conclusions

It is easy to compute a relative pseudo-acoustic impedance section from seismic data. To transform it to an absolute pseudo-acoustic impedance section, borehole acoustic impedance information is needed. We have a further possibility, i.e. the computation of another lithology parameter, porosity from an absolute pseudo-acoustic impedance section but more borehole information is indispensable for the computation and for checking the reliability of the results. If the reliability of the seismic porosity is good, it can greatly contribute to the reservoir delineation.

REFERENCES

Angeleri G. P., Carpi R. 1982: Porosity prediction from seismic data. Geophysical Prospecting, **30**, 5, pp. 580–607

Gardner G. H. F., Gardner L. W., Gregory A. R. 1974: Formation velocity and density – The diagnostic basics for stratigraphic traps. Geophysics, **39**, 6, pp. 770–780

Gogonenkov G. N., Krasavin Yu. V. 1983: Relationship between longitudinal wave velocity and density in sedimentary series. Geophysical Transactions, **29**, 3, pp. 203–216

Lindseth R. O. 1979: Synthetic sonic logs – a process for stratigraphic interpretation. Geophysics, **44**, 1, pp. 3–26

Maureau G. T. F. R., Van Wijhe D. H. 1979: The prediction of porosity in the Permian (Zechstein 2) carbonate of eastern Netherlands using seismic data. Geophysics, **44**, 9, pp. 1502–1517